Somatic Size and Cav1.3 Channel Expression in Vulnerable and Resistant Motoneurons of the SOD1 Mouse Model of Amyotrophic Lateral Sclerosis

Liza Shoenfeld

A thesis

submitted in partial fulfillment of the

requirements for the degree of

Master of Science

University of Washington

2013

Committee:

Prof. Marc D. Binder, Chair

Prof. Randall K. Powers

Prof. Stanley C. Froehner

Prof. William J. Spain

Program Authorized to Offer Degree:

Graduate Program in Neurobiology and Behavior

Table of Contents

REVIEW

AMYOTROPHIC LATERAL SCLEROSIS

Amyotrophic Lateral Sclerosis (ALS) is a progressive, fatal disease characterized by degeneration of motoneurons and loss of motor function. The most common adult-onset motoneuron disorder, ALS has a worldwide prevalence of approximately 2 per 100,000 people. While 5 – 10% of ALS cases are inherited in an autosomal dominant pattern, a full 90 – 95% are sporadic, with no known genetic component. Nevertheless, both the familial and sporadic forms of the disease present with a similar course of clinical features, supporting the hypothesis that they share pathological mechanisms (Cleveland and Rothstein, 2001).

ALS typically strikes adults between the ages of 50 and 70, with maximum incidence rates at age 65 (Kurtzke, 1982). The initial disease phenotype varies according to onset locality (spinal or bulbar) and the relative involvement of upper motoneurons versus lower motoneurons. Typically, patients present with some combination of muscle force loss, fatigue, difficulty swallowing, talking and/or walking, and spasticity. As the disease progresses, patients lose control of skeletal musculature, with the exception extraocular and pelvic muscles, which show remarkable resistance to degeneration. The cause of death is typically respiratory failure, within 3 – 5 years of diagnosis (Kiernan et al., 2011).

Nearly 150 years after Jean-Martin Charcot first described the disease, little is currently known about its cause or pathways. Nor is there a robust treatment: riluzole, the only drug currently administered to ALS patients, extends life by a matter of months (Lacomblez et al., 1996). The study of ALS is complicated by both the wide variance in clinical course as well as the multitude of mechanisms thought to be involved. The establishment of a genetic mouse model of the disease in the 1990s has allowed extensive inquiry into the presymptomatic development of this late-onset disease, but much remains to be determined about the selective and progressive degeneration of motoneurons in ALS.

Of patients with the familial form of ALS, 20% have a mutated form of the superoxide dismutase 1 (SOD1) gene, which encodes a protein that converts superoxide into hydrogen peroxide and is widely expressed throughout the nervous system (Crapo et al., 1992; Pardo et al., 1995). Missense mutations in the SOD1 gene were first reported in ALS families in 1993 (Rosen et al., 1993); since then over a hundred mutations in SOD1 and other genes have been linked to familial ALS (as reviewed in Turner and Talbot, 2008). In total, mutations in the SOD1 gene account for 2% of all ALS cases. While this represents only a small fraction of cases, it is to date the best available animal model for the study of ALS (Cleveland and Rothstein, 2001).

The pathology of the SOD1 mutant mouse closely mimics that of ALS. Mutant SOD1 is first expressed embryonically, but symptoms do not present until adulthood, allowing for the study of late onset pathology. Pathologies differ somewhat between mutant SOD1 variants, but all display the motoneuron loss in brainstem and spinal cord, neuromuscular junction denervation, and protein aggregates that are the hallmarks of ALS (Siklos et al., 1998a). Although the mechanism by which the SOD1 mutation causes motoneuron degeneration is still unknown, it likely involves a toxic gain of function rather than loss of function (Gurney et al., 1994).

Selective Motoneuron Vulnerability

The SOD1 gene is expressed in every cell in the body, but the protein produced by the mutated gene variant targets primarily motoneurons for degeneration (Pardo et al., 1995). Though the basis for this selective vulnerability is not fully understood, one important determinant might be cell size. With somatic diameters reaching over 50 um and extensive dendritic branching, motoneurons are among the largest cells in the body (Sherrington, 1899). Their large size reflects the heavy load of their functional responsibilities: the axon from a single motoneuron can branch out to

innervate hundreds of muscle fibers (Henneman et al., 1965), where motor commands are transduced to mechanical force.

Natural variation in motoneuron size creates a scale of activation thresholds governed by fundamental principles of electricity. The size principle put forth by Henneman describes a stereotyped process of recruitment in which motor units are progressively activated according to increasing axonal conduction velocity, and dismissed in mirrored order (Henneman, 1957). Motoneuron conduction speed is tightly correlated with axonal diameter, which in turn is proportional to the total membrane surface area, including the soma and dendritic branching. The link, then, between speed and recruitment order is motoneuron size. Ohm's law confirms that smaller neurons, which are characterized by higher resistance, experience a greater change in voltage than large neurons in response to the same current input.

Ordered recruitment governs not only the motoneuron activity, but also muscle fiber activation. Slowly conducting motoneurons tend to innervate a smaller number of slow twitch muscle fibers (Type I), allowing fine control of muscles generating weak force. Larger, faster motoneurons are responsible for activating a larger number of fast twitch, fatigue-resistant muscle fibers (Type IIa). The motor units producing the strongest force tend to consist of the largest motoneurons sending fast axons to a great number of fast twitch fatigable muscle fibers (Type IIb). Variety in conduction velocity exists within these classes as well, creating a spectrum of motor units accessible on a graded scale (Henneman et al., 1965).

Interestingly, motor unit failure in ALS mouse models follows an order opposite to that of recruitment, with the largest motor units degenerating first (Pun et al., 2006; Hegedus et al., 2007) . G93A mutant mice exhibit extensive local muscle denervation at p50, long before clinical onset at p90. In these mice, Type IIb fibers show the earliest synaptic loss at the neuromuscular junction, followed by Type IIa, with Type I synapses resistant to denervation (Frey et al., 2000a). Pun *et al*. (2006) also reported loss of Type IIb motor units first, followed by IIa and eventually Type I units in both the 93A and 85R models, though the authors argue that axons, not the neuromuscular junction or muscle fibers, are the site of vulnerability.

Loss of muscle force follows a similar pattern. Fast twitch muscles in male G93A mice undergo a selective decline in force and motor unit number by p40, 50 days prior to the onset of overt symptoms. In a second phase loss, slow twitch muscle contractile force weakens and motor unit number falls at p90, the time point at which G93A mice first present with tremors and patent weakness in the hindlimb muscles (Hegedus et al., 2007). An analysis of macro-EMG potentials and twitch contractions in ALS patients also reveals decreased twitch forces in motor units with higher thresholds when compared to controls (Dengler et al., 1990), though scant evidence exists in the literature to definitively support these findings (Eisen and Swash, 2001).

The disease progression of ALS thus prevents an interesting paradox: the largest motor units, which are employed far less frequently than smaller motor units, and require much greater levels of excitatory drive to activate, are the first to fail. What is it about larger size that confers greater vulnerability to ALS degeneration? How do smaller motoneurons resist degeneration during the early disease stages despite their frequent, repetitive activation? Much remains to be determined regarding the relationship between motoneuron size and vulnerability to ALS.

Clinical evidence has long suggested that specific subpopulations of motoneurons retain their functionality even late into the progression of ALS (Rosen, 1978). At end-stage, ALS patients usually retain control of eye movements and elimination functions, indicating sparing of the ocular and sphincter motoneurons (Charcot, 1874). However, difficulties in swallowing are a common early feature of the disease and are evident in nearly all patients (Kiernan et al., 2011) , suggesting universal deterioration of the hypoglossal nucleus. This selective susceptibility of specific subpopulations to the mutated SOD1 protein holds in animal models as well. Accordingly, the characterization of resistant and vulnerable motoneuron populations has become a major focus of study in the ALS field.

In the first quantitative evaluation of cranial motoneuron function in ALS patients, DePaul *et al.* (1988) reported greater weakness in voluntary muscle contraction of the tongue than of the lip or jaw muscles. The same pattern of non-

uniform cranial nerve deficiencies was seen across all patients, regardless of whether the disease initially presented as bulbar or nonbulbar. The authors conclude that ALS affects hypoglossal motoneurons to a greater extent, and earlier, than facial or trigeminal motoneurons.

Vulnerable motoneuron populations not only diminish in capacity to produce force, but also show morphological abnormalities. In autopsies of ALS patients, hypoglossal and spinal motoneurons show decreased size and increased circularity, while no physical changes are evident in the ALS-resistant nucleus of Onuf (Kiernan and Hudson, 1993). Sparing of the nucleus of Onuf in ALS patients has been well established (Iwata et al., 1978; Schrøder and Reske-Nielsen, 1984; Dubrovsky and Filipini, 1990; as cited in Kiernan and Hudson, 1993).

However, complexities in clinical presentations can complicate the distinction between vulnerable and resistant motoneuron populations. Comorbidity with other conditions, such as dementia, can result in degeneration of the oculomotor neurons, which are spared in typical ALS cases (Okamoto et al., 1993). Furthermore, advances in life support beyond the point of respiratory failure has revealed loss of oculomotor function in advanced stage patients (Hayashi and Kato, 1989). While this evidence points to the eventual vulnerability of ocular motoneurons, their resistance to degeneration through the majority of the disease course may give clues to therapeutic targets in ALS.

Selective motoneuron loss patterns in the SOD1 mouse models mirror those of the human disease condition. Cranial motor nuclei at endstage in the G93A mice show a massive loss of motoneurons in the hypoglossal, facial, trigeminal motor, and nucleus ambiguous in both histological (Nimchinsky et al., 2000; Haenggeli and Kato, 2002; Ferrucci et al., 2010) and in-vivo MRI examinations confirmed by post-mortem Nissl staining (Angenstein et al., 2004; Zang et al., 2004). Motoneuron loss is also evident in the G93A model at p90, the age of symptom onset, in both the trigeminal and hypoglossal nuclei (Haenggeli and Kato, 2002). In each of these

studies, ocular motor nuclei exhibit a motoneuron population density equal to that of wild type controls.

Evidence of motoneuron subpopulations resistant to ALS has prompted extensive investigation into the differences between vulnerable and resistant motoneurons. The first evidence for regulation of intracellular calcium levels as a key differentiator came from a postmortem study of ALS patients showing that resistant populations express higher levels of the proteins responsible for buffering intracellular calcium than vulnerable populations. Oculomotor and abducens motoneuron populations show immunoreactivity to the calbindin and parvalbumin calcium binding proteins, while immunoreactivity is absent in the cranial and spinal motoneuron populations affected early in the disease course. This relationship was confirmed using an in vivo cell culture model, in which vulnerability to cytotoxicity of ALS IgG correlated with the expression of these calcium binding proteins (Alexianu et al., 1994).

Motoneurons have a particularly low calcium buffering capacity, a property that endows them with more precise control of calcium signaling (Lips and Keller, 1998). Because calcium buffering capacity is directly proportional to the recovery time constant of cytosolic calcium levels, a low buffering capacity bestows a neuron with rapid recovery from calcium influxes (reviewed in Lewinski and Keller, 2005a). A calcium transient that is high in amplitude and decays quickly results in greater spatial and temporal definition of the calcium signal, and thus more precise control of the various calcium-dependent second messenger systems prevalent in motoneurons (Lips and Keller, 1998).

However, low calcium buffering capacity also confers greater vulnerability to calcium overload and its toxic consequences (Mattson et al., 1989). Indeed, within the motoneuron class, calcium binding ratios measured neonatally are 5-6 times lower in the vulnerable hypoglossal and spinal populations than in the resistant ocular motoneurons (Vanselow and Keller, 2000).

Whether intrinsic calcium binding capacities are further weakened in the mutant SOD1 motoneurons has yet to be conclusively determined. Lewinski *et al*. (2008) report a lower, but not significantly different, calcium binding ratio in the hypoglossal motoneurons of 2-4 day old G93A mice compared with WT. If mutant SOD1 does not affect calcium binding properties, the calcium overload characteristic of ALS is likely a result of increasing calcium loads rather than a reduced ability to process the calcium influx. However, these measurements of calcium buffering were performed at the neuron soma, not in the dendritic or axonal processes where most calcium enters (Carlin et al., 2000a). It remains to be seen if the SOD1 mutation leads to early alterations in intrinsic, cell-wide calcium binding capacities.

The effective increase in intracellular calcium concentration is governed by a number of factors, including calcium extrusion mechanisms, mitochondrial calcium sequestration, and buffering by calcium binding proteins (Patterson et al., 2007). Expression levels of these proteins correlate with vulnerability to degeneration in motoneuron populations (Elliott and Snider, 1995), making them a prime target of study. Indeed, expression patterns of the calcium binding proteins calbindin and parvalbumin mirror measured buffering capacities, indicating that calcium binding proteins may be the primary agents responsible for endogenous calcium buffering (Lewinski and Keller, 2005a).

Differential expression of calcium binding proteins distinguishes resistant and vulnerable motoneuron populations. In situ hybridization analysis of parvalbumin (PV) mRNA expression in rat motor neuron pools reveals that PV expression mirrors ALS susceptibility: robust synthesization of PV mRNA is evident in oculomotor and abducens motor neurons, but virtually no expression is seen in trigeminal motor, facial, hypoglossal, or limb motoneurons (Elliott and Snider, 1995). Laslo *et al.* (2000) examined expression patterns of calcium binding proteins and found expression of parvalbumin in oculomotor but not hypoglossal motoneurons. However, the authors also reported parvalbumin labeling in vulnerable spinal motoneurons, suggesting that immunoreactivity of calcium binding proteins may not always be a reliable marker for resistance to ALS.

This differential expression of calcium binding proteins between vulnerable and resistant populations is tied to measurable consequences for neuron health. In a G93A SOD1 mouse, spinal motoneuron cell bodies and proximal dendrites which lack parvalbumin show degeneration, vacuole formation, and increased intracellular calcium levels at P60, while none of these changes are evident in the parvalbumin-rich oculomotor neurons of the same age (Siklos et al., 1998b). In a study of response to neuronal injury, axotomized oculomotor neurons of adult WT mice exhibit a brief calcium increase and upregulation of parvalbumin expression, whereas axotomized hypoglossal motoneurons show a larger and more prolonged increase in intracellular calcium but no change in parvalbumin levels. Here, the ability to upregulate parvalbumin is protective against calcium toxicity after injury. (Obál et al., 2006).

Indeed, overexpression of calcium binding proteins can be protective against SOD1-induced degeneration. Cells transfected with calbindin exhibit lower calcium entry through voltage gated calcium channels and are better able to mitigate calcium transients evoked by voltage depolarizations than WT cells (Lledo et al., 1992). In a genetic model, SOD1 mice crossed to an overexpressing parvalbumin mouse (PV+/+) show significantly less motoneuron death, delayed disease onset, and prolonged survival. Further analysis shows that parvalbumin overexpression protects by mitigating toxic calcium influx: ALS immunoglobins increase intracellular calcium at motoneuron terminals in wild type controls, but not in mice overexpressing parvalbumin (Beers et al., 2001). SOD1 mice overexpressing parvalbumin also exhibit greater resilience to calcium toxicity after injury. In the standard SOD1 model, axotomized hypoglossal motoneurons show a transient increase in intracellular calcium after injury, but mice overexpressing parvalbumin show no such increase (Paizs et al., 2010)

Persistent inward currents endow motoneurons with the capacity for self-sustaining activation in response to any input, however brief, that elevates the membrane potential to the activation voltage of the PIC channels (reviewed in Heckman et al., 2008). The PIC is generated by slowly inactivating voltage-gated channels, which allow for prolonged plateau potentials that promote cell excitability even after the cessation of the initial synaptic input. These PIC channels, whose activity is heavily influenced by descending monoaminergic input, are essential to the bistability that characterizes motoneuron firing patterns (Hounsgaard and Mintz, 1988).

In mammals, extensive *in vivo* and *in vitro* work has demonstrated that the PIC is composed of two distinct conductances: fast-activating persistent Na channels give rise to a leading inward sodium current (Lee and Heckman, 1999), while Ca channels generate a slow-activating inward calcium current (Schwindt and Crill, 1980). The Ca-PIC and Na-PIC perform complementary functions to produce an accessible and sustained depolarizing force. The Na-PIC, which has a lower activation threshold, is largely responsible for enabling spike initiation. However, this current activates and inactivates too rapidly to generate the sustained depolarization necessary for a stable firing state. The Ca-PIC, slower to inactivate, once engaged is a persistent source of inward current (Hounsgaard and Kiehn, 1989). Accordingly, the fast activating Na-PIC may serve as a bridge to the sustained activation of the Ca-PIC (Li et al., 2004).

This review will focus on the Ca-PIC and its associated channels. Not only is Ca-PIC responsible for the majority share of persistent inward current (Powers and Binder, 2003), it also contributes appreciably to calcium influx (Choi, 1988). Carlin *et al.* (2000) were the first to demonstrate that, in functionally mature mammalian motoneurons, this current is mediated primarily by dendritically located L-type calcium channels. The molecular subtype has since been identified as the Cav1.3 L-

type calcium channel (Li and Bennett, 2003). Whereas L-type channels are typically classified as high-voltage activated (Umemiya and Berger, 1994), the Cav1.3 subtype have an unusually hyperpolarized activation threshold that indicates they likely mediate calcium influx and its resulting processes in response to relatively minor membrane depolarizations (Xu and Lipscombe, 2001).

The problem of localizing the calcium-mediated persistent inward current within the motoneuron is compounded by the inherent bias of many experimental methods. Schwindt and Crill (1980), for example, were among the first to identify a calcium-mediated persistent inward current in the vertebrate motoneuron, but the somatic voltage clamp used to characterize this current complicates spatial profiling of the responsible calcium conductances. The authors proposed that a local, voltage-controlled conductance is responsible for the observed plateaus, though they acknowledge that an electrotonically distal conductance, outside the control of voltage clamp, may allow for the propagation of distally generated currents

Using a differential polarization technique applied to motoneurons in turtle spinal sections, Hounsgaard and Kiehn (1993) demonstrated the capacity for distal dendrites to generate calcium-mediated plateau potentials. However, the limited spatial resolution of this technique precludes any further insight into the distribution pattern of the responsible channels, beyond confirming that they are present in both the soma and electronically distant dendrites.

The dendritic contribution to plateau potentials was confirmed *in vivo* through a voltage clamp protocol in which a depolarized holding potential both nonlinearly amplifies Ia effective synaptic current, and prolongs the ensuing tail current. The authors contend that such behavior is the result of noninactivating calcium currents residing in the dendrites, though a somatic component cannot be ruled out (Lee and Heckman, 1996).

The L-type calcium channel that mediates the Ca-PIC has since been localized to the dendrites of mammalian spinal motoneurons using whole-cell patch clamp recordings, and confirmed through immunohistochemical analysis. With sodium

and potassium currents blocked, spinal motoneurons demonstrate delayed onset, dihydropyridine-sensitive current, as well as large tail currents, consistent with an inward conductance that is electrotonically distant to the somatic site of voltage control. Polyclonal antibody labeling of the alpha-1D subunit reveals particularly strong expression of Class D L-type Ca channels in dendritic membrane beyond the second or third branch point, but not in somatic or proximal dendritic membrane. Here, the evidence supports a dendritic origin for the persistent calcium current that endows motoneurons with bistability (Carlin et al., 2000b).

Notably, the anatomical and physiological development of L-type calcium channels corresponds with the progressive gain of motor function in postnatal development. In the isolated mouse spinal cord, the L-type calcium channel blocker nifedipine has no effect on chemically induced rhythmic bursting in motoneurons of animals less than one week old, but reversibly inhibits this bursting in animals seven days and older (Jiang et al., 1999b). The onset of functionality in L-type calcium channels at P7 coincides nicely with the emergence of walking and weight-bearing behaviors, evident at P9-10 in these mice (Jiang et al., 1999a). Indeed, the parallel development of Ca-PIC and higher order motor function lends further evidence to dendritic, voltage-gated calcium channels as the mediators of motoneuron bistability (Carlin et al., 2000b).

Immunohistochemical evidence also supports the progressive postnatal development of L-type calcium channels. Labeling patterns for the Alpha 1C and 1D subunits grow from weak peri-nuclear labeling at P2, to significant cytoplasmic labeling at P10-11, and reach full adult labeling patterns by P18-19 (Jiang et al., 1999b).

Cranial motoneurons also show use-dependent development of the voltage-gated calcium channels (VGCC) underlying the persistent inward current. In Wistar rats, as oculomotor motoneurons acquire functionality at approximately P14, they also show a market decrease in the VGCC current density as compared to oculomotor motoneurons from nonvisual neonatal rats. Interestingly, the

hypoglossal motoneurons, which support motor behaviors functional from birth, show no change in calcium current densities between neonatal and juvenile time points (Miles et al., 2004). How the differential calcium channel development patterns between these vulnerable (hypoglossal) and resistant (oculomotor) might be hijacked by the SOD1 mutation in ALS has yet to be investigated.

Presymptomatic Pathology

A number of abnormalities in ALS can be detected before symptom onset, including: increased neuronal excitability, increased neuronal size, impaired axon transport, alterations in glutamate receptors, deficits in mitochondrial function, protein ubiquitination, and impaired calcium buffering (reviewed in Redler and Dokholyan, 2012). Examining pathological events that take place prior to the onset of overt symptoms is crucial in the study of ALS, since in the familial form, mutations are genetically encoded from birth, yet normal function persists until late in adulthood. Mutant SOD1 mouse models provide an opportunity to study presymptomatic changes in a late onset disease beginning at the embryonic stage. This section will focus on evidence for aberrant physiological and structural changes in mSOD1 motoneurons.

Elevated intrinsic excitability is one of the earliest known alterations in mSOD1 motoneurons (Pieri et al., 2003). Cultured G93A spinal motoneurons from both embryonic and neonatal stages exhibit elevated maximal firing rates and a steeper F-I gain when compared to WT spinal motoneurons (Kuo et al., 2004). This hyperexcitability is proposed to reflect an intrinsic aberration of the motoneuron, since the AHP shows no deviations and synaptic transmission was blocked in the protocol. While the culture model permits evaluation of neurons in their infancy, the authors acknowledge that this paradigm isolates motoneurons from influential factors, such as the Ca-PIC (Kuo et al., 2005).

Work in the slice preparation supports the finding of early intrinsic hyperexcitability in mSOD1 motoneurons. In a whole cell patch clamp comparison of electrophysiological properties, p6-10 G93A lumbar motoneurons exhibit a more depolarized resting membrane potential, lower rheobase current, wider and smaller spike potentials, a longer AHP, and a greater F-I gain than their WT counterparts (Pambo-Pambo et al., 2009). Early hyperexcitability in mSOD1 motoneurons is further supported by evidence from hypoglossal motoneurons of p4-10 G93A mice showing enhanced frequency of spontaneous excitatory and inhibitory transmission and increased AP amplitude (van Zundert et al., 2008).

However, conflicting evidence complicates an otherwise straightforward finding. In various studies of the electrophysiological properties of mSOD1 motoneurons, the AHP has been reported as shorter than (Quinlan et al., 2011), longer than (Pambo-Pambo et al., 2009), and not different from that of WT counterparts (Kuo et al., 2004; van Zundert et al., 2008). The action potential has been found shorter in duration (Quinlan et al., 2011), wider and smaller (Pambo-Pambo et al., 2009), and unchanged in threshold and duration (Kuo et al., 2005; Bories et al., 2007; van Zundert et al., 2008). The F-I slope of mSOD1 motoneurons has at times been reported as steeper (Kuo et al., 2004; Pambo-Pambo et al., 2009), less steep (Bories et al., 2007), and equal to its WT counterparts (Quinlan et al., 2011).

Reconciling these contradictory reports is a challenging task made more difficult by variations introduced through motoneuron population and mSOD1 variant. Normal brainstem motoneurons, for example, differ from normal spinal motoneurons in the ontological development of F-I gain: gain decreases with age in spinal motoneurons (Meehan et al., 2010), but increases with age in brainstem motoneurons (Carrascal et al., 2005 as cited in Quinlan et al., 2011). Accordingly, a steeper gain in spinal motoneurons may indicate pathological hyperexcitability, but in brainstem motoneurons may simply be indicative of accelerated maturation.

Given that the two most commonly studied mSOD1 variants differ widely in the time course of disease progression, it follows that motoneurons affected by these mutated proteins would also demonstrate distinct profiles of physiological changes. The G85 variant, which exhibits a latency to disease onset nearly twice as long as the G93A variant (Bruijn et al., 1997), has been shown to have both reduced excitability p10, (Elbasiouny et al., 2010); p6-10 (Bories et al., 2007), and no difference in excitability when compared to WT motoneurons p6-10 (Pambo-Pambo et al., 2009). Pambo-Pambo *et al.* (2009) notes that the discrepancy between these findings and those of hyperexcitability in the G93A line could result from different timing of developmental processes and compensatory mechanisms and/or from distinct toxic properties of the mutated proteins.

While the ontological profile of altered excitability remains to be conclusively established, clinical data suggests hyperexcitability is a component of the disease progression. ALS patients show an increased stimulus-response curve to transcranial stimulation in motor cortex (Zanette et al., 2002), which may reflect either an increase in excitability of corticospinal neurons or spinal motoneurons, or a combination of both (Kuo et al., 2005).

Although there are conflicting findings regarding the nature of mSOD1-induced changes in excitability, all available evidence points to an increase in persistent inward current in SOD1 motoneurons. Indeed, changes to the PICs in mSOD1 motoneurons are among the earliest recorded abnormalities in the disease model (Kuo et al., 2005).

In cultured G93A spinal motoneurons (e12-14), the sodium component of the PIC is enlarged in both high and low input conductance neurons. However, the greater Na-PIC only results in the larger overall PIC in high input conductance cells, because low input conductance neurons produce a compensatory outward shift in the TTX-insensitive PIC (Kuo et al., 2005). This finding provides one possible pathway through which large motoneurons are selectively vulnerable to the toxic effects of mSOD1: though all motoneurons experience an upregulation in the PIC,

small motoneurons evade the pathology of enhanced excitatory tone through either a compensatory increase in outward potassium current or decrease in inward Ca-PIC. Lacking in this embryonic cell culture model, though, is an understanding of the contribution of L-type calcium channels to the PIC profile.

The calcium component of the PIC develops later than the sodium component (Jiang et al., 1999b), and there is evidence to suggest that the SOD1 mutation results in both a greater Ca-PIC amplitude in juvenile mice (Quinlan et al., 2011) as well as a greater Na-PIC amplitude in neonatal mice (van Zundert et al., 2008; Quinlan et al., 2011). The increase in Na-PIC appears to occur without any corresponding increase in the density of Na channels. The authors suggest that an enhancement of Na-PIC may instead result from a premature Na channel isoform turnover to isoforms that permit greater levels of persistent activity (van Zundert et al., 2008)

Finally, Quinlan *et al.* (2011) argue that the expected hyperexcitability produced by early upregulation of the PIC in mSOD1 motoneurons is instead mitigated by changes in size and specific input conductance (Amendola and Durand, 2008; Elbasiouny et al., 2010; Quinlan et al., 2011). Under this logic, it follows that motoneurons have only a limited capacity for such reactionary changes, past which it will eventually succumb to toxicity mediated either through elevated PIC and/or increased cell size.

Because large, high input conductance neurons require higher levels of excitatory synaptic input to reach firing threshold (Henneman, 1957), a compensatory enlargement of neuronal size may stave off the effects of hyperexcitability, at least temporarily. Of interest to researchers is whether motoneurons undergo transformations in size or shape in response to the disease progression, and whether these transformations relate to changes in physiological properties. This section will review anatomical and physiological evidence for structural changes to soma and dendrites, as well as degenerative and compensatory changes to axonal processes.

Morphological evaluations of soma size indicate no differences between WT and mSOD1 motoneurons at the neonatal (Amendola and Durand, 2008) or embryonic stages (Kuo et al., 2004). However, electrophysiological assessments have shown elevated input conductance and reduced capacitance in neonatal mSOD1 motoneurons, indicative of enlarged size {Bories:2007cl}.

Quinlan *et al.* (2011) reported that WT lumbar motoneurons exhibit an increase in conductance between the age groups of p0-5 and p6-12, but that in the mSOD1 line, this increase is significantly larger. Interestingly, it appears that this shift is not distributed equally among all sizes of motoneurons. Bories *et al.* (2007) found that the lower average input resistance of the SOD1 group results not from a full population shift, but from a selective effect in the subpopulation of neurons with an already low resistance. The largest motoneurons, it seems, are specifically vulnerable to enlargement quite early in the disease progression.

If somatic sizes remain equal between mSOD1 and WT neonatal motoneurons, but electrophysiological data points to increased neuronal size, it follows that the dendritic tree may be the locus of morphological changes. Indeed, neonatal lumbar motoneurons of G85R SOD1 mice show greater dendritic branching, greater dendritic length, more branching nodes, and greater total dendritic surface area than WT mice (Amendola and Durand 2008). While there is no difference in number or mean diameter of primary dendrites, these data do suggest that the mutated SOD1 protein leads to abnormal dendritic growth, perhaps through a deficit in pruning mechanisms or a misbalance between excitatory and inhibitory inputs (Amendola and Durand, 2008).

Evidence from computer modeling supports the same conclusion: simulations based on experimental data show that increases in dendritic membrane surface area and branching are responsible for one third of the reduction in input resistance. Decreased specific membrane resistance accounts for the remaining two thirds. The authors argue that as a consequence of reduced input resistance, affected motoneurons become more difficult to recruit, resulting in a loss of muscle control.

Furthermore, they propose that this reduction in muscle activity may then lead to retraction of axons and neuronal degeneration (Elbasiouny et al., 2010).

Axonal denervation and loss of motor units are well established pathological events in the ALS disease course (Hanyu et al., 1982; Bjornskov et al., 1984; Gurney et al., 1994a; Fischer et al., 2004). When loss of the neuromuscular junction leads to muscle denervation, intact axons sprout to open sites in a compensatory attempt to regain control of the muscle (Frey et al., 2000b). Collateral reinnervation is initially quite successful at maintaining normal twitch tension (McComas et al., 1971), but eventually is overtaken by the severity of degeneration (Gurney et al., 1994a).

There is evidence for axon degeneration prior to the onset of symptoms in mSOD1 mice. Fischer *et al.* (2004) reported that at p47, more than 30 days before symptom onset in the G93A mouse, 40% of endplates are denervated. Severe motor axon loss follows between p47 and p80, with notable loss of motoneuron cell bodies from the lumbar spinal cord after p80. This finding is in agreement with several other studies reporting loss at the NMJ prior to symptom onset (Kennel et al., 1996; Schaefer et al., 2005; Pun et al., 2006).

Interestingly, motor unit type appears to govern axon susceptibility to degeneration. Frey *et al.* (2000a) also found extensive local muscle denervation at p50 in the G93A mouse, but showed that loss follows a size ordered pattern: type IIb are the earliest affected fibers, followed by type IIa, with synapses on type I fibers resistant to denervation. Furthermore, Hegedus *et al.* (2007) report a biphasic pattern of loss in which motor unit numbers decline dramatically in fast twitch muscles between birth and p60. Following a plateau period, motor unit numbers in slow twitch muscles proceed to fall beginning at p90. From these data, it appears that slow motor neurons are more resistant than fast ones to the toxic effects of mSOD1.

The capacity for collateral reinnervation of denervated NMJ targets by surviving axons is well established in both ALS and mSOD1 models (McComas et al., 1971; Mulder and Howard, 1976; Hanyu et al., 1982; Bjornskov et al., 1984; Gurney

et al., 1994a; Kennel et al., 1996). However, the degree to which this compensation leads to functional gain is somewhat contested.

Evidence from mSOD1 mice suggests a pattern in which the initial degeneration of FF axons prompts collateral sprouting by remaining FR and S axons, leading to a temporary recovery before escalating degeneration proves insurmountable (Frey et al., 2000a; Fischer et al., 2004; Pun et al., 2006). Using retrograde tracers, Millecamps *et al.* (2001) showed that denervation-induced sprouting at the NMJ actually enhances the uptake capacity of G93A motoneurons in symptomatic mice. The surprisingly high level of tracer uptake from muscle to motoneuon suggests that newly sprouted compensatory axons are indeed functional, and may contribute to a transient recovery.

Clinical evaluations support this theory. Some ALS patients show a temporary improvement in muscle tone and force after the disease onset (Mulder and Howard, 1976), which may be due to successful collateral reinnervation (Kennel et al., 1996). Furthermore, in patients suffering from various types of chronic motor denervation, muscles which have lost nearly 90% of motor units can still exert twitch tensions within the normal range. This observation clearly indicates that surviving motor units can compensate for denervation by developing a far greater tension capacity (McComas et al., 1971).

Hegedus *et al.* (2007), however, contend with the proposal that compensatory sprouting is robust or functional. They describe a parallel decline in motor unit numbers and whole muscle contractile force in hindlimb muscles of the G93A mouse between 40 and 120 days of age. A corresponding decrease in muscle force with motor unit number does not support functional compensatory motor unit expansion. Future work is required to reconcile this result with others in mSOD1 mice and ALS patients that do indicate functional compensatory sprouting.

Calcium-Mediated Mechanisms of Toxicity

The involvement of calcium in the pathology of ALS has been well established (Alexianu et al., 1994; Sikl s et al., 1996; Siklos et al., 1998a). The mechanisms through which calcium exerts its toxic effects, however, are less well understood. Calcium is likely an instigator of an interconnected web of pathological events that include glutamate excitotoxicity, aberrant mitochondrial function, and impaired axonal transport. The timing and order of these processes has yet to be firmly established; also lacking is an understanding of which event(s) is the initial instigator of degeneration. This section will provide a brief overview of calcium-mediated mechanisms thought to underlie motoneuron degeneration in ALS while pointing the reader to additional reviews for more comprehensive discussions.

Excessive glutamate exposure results in well documented short and long-term neurotoxic effects (reviewed in Shaw and Ince, 1997)). In ALS, several lines of evidence support a self-propagating destructive loop in which glutamate overexposure induces intracellular calcium overload, which in turn contributes to further sensitization to glutamate (Novelli et al., 1988). Motoneurons, which receive high levels of glutamatergic input (Shaw and Eggett, 2000), are particularly vulnerable to excitotoxicity (Regan and Choi, 1991). The mechanisms of glutamate toxicity in motoneurons are not fully established, but may involve calcium-dependent pathways. Here, the relationship between glutamate toxicity, calcium, and ALS pathology is discussed. For a more comprehensive review, see (Shaw and Ince, 1997).

A report of elevated glutamate levels in the cerebrospinal fluid of postmortem ALS patients first exposed excessive extracellular glutamate as a potential mediator of ALS pathology (Rothstein et al., 1990). One contributing factor to excessive extracellular glutamate may be decreased uptake capacity in the diseased system. In ALS patients, glutamate uptake speed is diminished in synaptosomes from the spinal cord, motor cortex, and somatosensory cortex, but

not in regions unaffected by ALS, like visual cortex, striatum, or hippocampus (Rothstein et al., 1992).

A number of distinct glutamate transporters remove glutamate from the extracellular space. Of these, the astroglial GLT-1 (EAAT2) is the transporter responsible for the majority of glutamate uptake (Pines et al., 1992; Bruijn et al., 1997). It follows that a loss of GLT-1 activity may underlie the decreased reuptake capacities observed in the synaptosomes of ALS patients. Indeed, ALS patients show a pronounced loss of GLT-1 both in spinal cord and motor cortex (Rothstein et al., 1995), a finding confirmed in the mutant animal disease model (Bruijn et al., 1997).

Chronic blockade of GLT-1 synthesis, both *in vivo* and *in vitro*, produces elevated extracellular glutamate levels, excitotoxic neurodegeneration, and progressive paralysis (Rothstein et al., 1996). Conversely, pharmacological upregulation of GLT-1 expression protects against motoneuron loss and extends survival times in the mSOD1 mouse (Rothstein et al., 2005). GLT-1 upregulation also lessens the calcium overload response to glutamate exposure (Liu et al., 2013). Together, these findings point to a key role for GLT-1 in the pathological processes of ALS.

GLT-1 may in fact be a direct target of the ALS-linked mutant SOD1 protein. Induced oxidative stress selectively targets GLT-1 in SOD1 mutants. In oocytes expressing mutant, but not WT SOD1, elevated hydrogen peroxide specifically inactivates this glutamate transporter (Trotti et al., 1999). These findings raise an intriguing possibility: mSOD1 may instigate multiple simultaneous challenges to neuronal equilibrium, at once enhancing excitability, while also interfering with the neuron's capacity to recover from excitation.

Overexposure to the excitatory amino acid glutamate, whether through elevated extracellular levels or impaired uptake at the cleft, triggers a number of destructive pathways. Acutely, depolarization induces an influx of water, sodium and chloride ions, causing a neuronal swelling that is reversible in cases of modest excitotoxicity, but likely pathological under prolonged duress (Choi, 1987). In a

second stage, excessive stimulation of glutamate receptors instigates an influx of calcium through glutamate receptor ionotropic channels AMPA (Van Den Bosch et al., 2000; Corona and Tapia, 2007) and NMDA (Liu et al., 2013), as well as voltage-gated calcium channels (Miller et al., 1989).

The resulting destabilization of intracellular calcium homeostasis activates a cascade of destructive biological events including overactivation of numerous enzyme systems (Urushitani et al., 1998) and the subsequent overproduction of reactive oxygen species (Carriedo et al., 2000). A neuron unable to regulate intracellular calcium levels is also vulnerable to activation of endoplasmic reticulum stress response (Bernard-Marissal et al., 2012), and deficits in mitochondrial energetic metabolism (Corona and Tapia, 2007), though whether apoptotic pathways are triggered as a result is contested (Bendotti et al., 2001).

Interestingly, the primary pathological processes activated by excitotoxicity can result in a secondary toxicity with long-term effects. Initial injury to mitochondrial function and ATP production via elevated intracellular calcium can disrupt the energy gradient needed to produce a normal resting membrane potential. Under depolarized membrane potentials, the NMDA receptor channel loses its voltage-dependent Mg block, resulting in an over-activation of NMDA receptors even by normal glutamate levels (Novelli et al., 1988). This study shows that glutamate toxicity self perpetuates: initial excitotoxicity induces sensitization to further excitatory input.

As further evidence for excitotoxicity as a primary mechanism for ALS pathology, the only drug shown to be effective in delaying the disease, acts by interfering pre- and postsynaptically with glutamate neurotransmission (Estevez et al., 1995). Riluzole treatment can increase survival by 35% at 18 months in ALS patients (Lacomblez et al., 1996) while also ameliorating the loss of muscle strength (Bensimon and Lacomblez, 1994). In the animal model of ALS, riluzole prolongs survival but does not delay disease onset (Gurney et al., 1996).

Riluzole exerts its protective effect via a blockade of both glutamate release and voltage-sensitive sodium channels on glutamatergic nerve terminals. Specifically, the drug blocks NMDAR activity, but is less effective at preventing kainite and AMPAR-mediated neurotoxicity (Estevez et al., 1995). Shaw and Ince (1997) note that the binding affinity of riluzole is substantially higher for the inactivated state of the sodium channel than for the activated state. The drug preferentially targets neurons whose sodium channels are more likely to be in the inactivated state.

With low capacities for cytosolic calcium buffering, motoneurons rely heavily on calcium buffering by mitochondria (Lautenschläger et al., 2013). In hypoglossal motoneurons, mitochondria participate in calcium uptake and clearance at intracellular calcium concentrations much lower than those observed for other neuron types. Mitochondrial calcium uptake is minor, however, in highly buffered, ALS-resistant motoneuron populations, suggesting a compensatory increase in mitochondrial buffering in neurons with low cytosolic buffering capacity (Lewinski and Keller, 2005b).

Not only does mitochondrial buffering take on the majority of the calcium burden in neurons susceptible to ALS, but recent evidence suggests that the disease impairs this essential process. Mitochondria isolated from brain and spinal cord motoneurons of mutant SOD1 mice display impaired calcium capacity as early as p35, prior to the onset of symptoms. No such reduction in calcium capacity was reported in mitochondria isolated from the liver, a non-affected tissue. That abnormal mitochondrial calcium handling arises early in the disease course suggests it may contribute to accelerating cell damage and later onset excitotoxic damage (Damiano et al., 2006).

However, the extent to which mitochondrial calcium buffering capacity determines disease course has recently been debated. By eliminating ubiquitous expression of cyclophilin D, a regulator of calcium-mediated opening of the mitochondrial permeability transition pore that gates calcium entry, Parone *et al.*

(2013) demonstrated that a robust increase in mitochondrial calcium buffering in mutant SOD1 mice reduces neuron loss, mitochondrial swelling, SOD1 protein misfolding and aggregation, and glial activation. Despite these gains, no changes were observed in muscle denervation, motor axon denervation, or disease progression and survival. Accordingly, the authors posit that mSOD1-mediated loss of mitochondrial calcium buffering capacity is not a primary disease mechanism of ALS.

Evidence for the involvement of mitochondria in ALS disease pathology came first from studies citing abnormal histological mitochondrial profiles, like swelling and vacuolation, in both ALS patients (Sasaki and Iwata, 1996a) and SOD1 models (Wong et al., 1995; Kong and Xu, 1998; Martin et al., 2006). Indeed the first direct demonstration of altered calcium levels in ALS showed that this elevated intracellular calcium was found enclosed in organelles, largely mitochondria, and resulted in a notable swelling of the mitochondrial body (Sikls et al., 1996).

Evidence suggests that mitochondrial damage is presymptomatic, and emerges very early in the fast-progressing mSOD1 models. At 2 weeks of age, G93A SOD1 mice show mitochondrial swelling and microvacuolation in the cytoplasm of fast-fatigable motoneurons (Bendotti et al., 2001). The precise mechanism through which mitochondrial damage contributes to ALS pathology is still unknown, but does involve a negative cycle in which calcium overload damages mitochondria, which in turn further sensitizes mitochondria to glutamate and glutamate-induced calcium overload (as reviewed in Lewinski and Keller, 2005a).

Axonal Transport

The accumulation of neurofilaments in the cell body and proximal axons is a hallmark of ALS pathology (Munoz et al., 1988; Sasaki and Iwata, 1996b), suggesting aberrations in, or an imbalance of, anterograde and retrograde axonal transport (De Vos et al., 2007). Given that retrograde and anterograde axonal transport are accomplished by distinct sets of structural entities (Tsukita and Ishikawa, 1980), it

is entirely possible that the disease mechanisms of ALS affect these directional systems differentially.

The effect of mutant SOD on fast axonal transport, in both the anterograde and retrograde directions, remains under contention. In a muscle biopsy study of severely affected ALS patients, (Breuer and Atkinson, 1988) reported both a decrease in the speed of retrograde organelle trafficking as well as an increase in axon transport speed in the anterograde direction. The faster anterograde speed, the authors argue, reflects a compensatory increase in the motor unit size of surviving motoneurons as surrounding motoneurons are progressively lost. Growth in the reach of a motor unit in turn increases the demand for neurotransmitters and other factors packaged in membrane-bound organelles. Here, an increase in organelle trafficking speed may be simply a compensatory response to higher demand (Breuer and Atkinson, 1988). In agreement, Dupuis *et al*. (2000) report an upregulation of a factor responsible for fast anterograde axonal transport in a mutant SOD1 mouse, though expression returns to control levels as the disease progresses.

To the contrary, multiple studies in both ALS patients (Sasaki and Iwata, 1996b) as well as mSOD1 models (Zhang et al., 1997; Warita et al., 1999; Lewinski and Keller, 2005b; De Vos et al., 2007) report an impairment in anterograde axonal transport. A disruption in anterograde transport, shown in the motoneurons of both presynaptic mice and embryonic culture, may cause loss of neurotransmitter release, metabolic dysfunction at the terminals, and accumulation of cytoplasmic neurofilaments (De Vos et al., 2007).

Regarding retrograde axonal transport, the literature is in agreement: organelle transport speed is slower in both ALS patients (Breuer and Atkinson, 1988) and SOD1 models (Lewinski and Keller, 2005b; De Vos et al., 2007). Loss of retrograde transport capacity interrupts the transmission of trophic factors from neuromuscular targets back to innervating motoneurons. Without trophic support, motoneurons are likely to exhibit the denervation typical of ALS (Frey et al., 2000a).

Interestingly, calcium also appears to play a role in the modulation of fast axon transport. Calcium channel agonists increase the speeds of both anterograde and retrograde fast axonal transport in motoneurons (Larivière and Lavoie, 1982; Breuer and Atkinson, 1988), likely not through direct action on transport motors or organelles, but rather through indirect modulation of cytoskeletal elements (Breuer et al., 1992). Neuron cell bodies incubated in calcium-free buffer show reduced axonal transport of protein, though transport is unaffected by exposure of neuron trunks to calcium-free conditions (Hammerschlag et al., 1975).

Motoneurons rely on axonal trafficking of mitochondria to the neuromuscular junction, where they process the rapid calcium fluctuations associated with active synapses (reviewed in Redler and Dokholyan, 2012)). Given that trafficking of mitochondria is particularly impaired in SOD1 mice (De Vos et al., 2007), one plausible scenario is that impaired mitochondrial trafficking results in accumulation of mitochondria in proximal axons (Sasaki and Iwata, 1996b), as well as a loss of mitochondrial calcium buffering support in distal axons. This explanation is supported by evidence that distal axonopathy is an early and pervasive feature in both ALS patients and SOD1 models (Fischer et al., 2004). However, the precise mechanisms through which calcium acts on axonal transport, as well as the interactions between ALS pathology, calcium dynamics, and transport remain to be determined (Mórotz et al., 2012).

Disease Progression

Despite a hundred and fifty years of clinical observation, and an extensive body of scientific literature, the pathogenesis of ALS remains frustratingly elusive. The study of the disease is complicated by a number of factors, including: limited genetic models to mimic the familial form of the disease, a poor understanding of susceptibility genes involves in the sporadic form, the diversity of clinical presentations, comorbidity with other degenerative diseases, and the long

prodromal period that separates disease onset from presentation of symptoms (as reviewed in Kiernan et al., 2011).

Of these, the delayed onset of disease symptoms presents a particularly challenging problem to researchers seeking to establish a theory of disease progression. Because the initial target(s) of the disease are still unknown, separating the primary disease process from the secondary effects and compensatory mechanisms that follow is exceedingly difficult. Since the establishment of a mouse line expressing mutant SOD1 protein over 15 years ago (Gurney et al., 1994b), a host of early abnormalities, some even in the embryonic stage, have been reported in the murine line (van Zundert et al., 2012). Given that these pathological changes are initiated long before the onset of symptoms, one model postulates that a very early pathogenesis triggers a number of compensatory mechanisms which mask primary events, but that as the animal ages, the eventual saturation of compensatory mechanisms results in degeneration and death (van Zundert et al., 2008; 2012).

How aging affects disease penetrance is also unknown, but three models have been proposed by Chiu *et al*. (1995) in the first report of the mutant SOD G93A line. First, in the stochastic model, damage accumulates with age until reaching a threshold that triggers outward disease expression. Second, a senescence model proposes that protective mechanisms fail with age, allowing disease expression. Third, genetic changes in aging cells may permit increasing penetrance of the disease. Of these, the authors favor the first hypothesis, in which neurons tolerate pathological changes until a point is reached at which normal function is no longer possible. Verifying this hypothesis, however, will likely require the distinction of primary versus secondary pathological events.

The difficulty of determining the initiation and sequence of pathology has also led to two competing theories of disease progression: the “dying forward” and “dying back” hypotheses. Though both view motoneuron death as a secondary consequence of an earlier, primary pathology, they differ in the origin of that initial

event. Proponents of the dying forward hypothesis argue that cortical hyperexcitability propels injury forward to the motoneuron (Trotti et al., 1999; Vucic, 2006), while the dying back hypothesis postulates that degeneration at the neuromuscular junction initiates pathologies that move retrogradely back to the motoneuron (Frey et al., 2000a; Gould, 2006).

Support for the dying forward hypothesis comes primarily from clinical observations of hyperexcitability in cortico-motoneurons. Patients suffering from motoneuron disease show a reduction in short interval intracortical inhibition, as measured through transcranial magnetic stimulation. This loss of inhibition may be explained either by a loss of inhibitory cortical motoneurons, or a glutamate-mediated downregulation of inhibitory activity (Vucic, 2006). In the mouse model, young (2-3 week) mSOD1 mice show reduced GABAergic inhibition in layer 5 pyramidal neurons, providing support for a cortical hyperexcitability that precedes symptom onset (Nieto-Gonzalez et al., 2011). That the ALS drug riluzole acts by interfering with glutamate transmission provides further support for this hypothesis (Estevez et al., 1995).

To the contrary, the dying back hypothesis proposes a pathology that originates at the junction between the motoneuron axon terminal and the target muscle, or at the target muscle cells themselves. A number of studies have demonstrated degeneration or dysfunction of NMJ elements prior to loss of motoneuron cell bodies in mSOD1 mice. Physiologically-detectable loss of entire motor units begins as early as p40 (Kennel et al., 1996), while immunocytochemical analysis shows loss of synapses pertaining to fast firing motor units at p50 (Frey et al., 2000a). In a spatiotemporal analysis of motoneuron pathology, denervation at the neuromuscular junction is evident by p47 and loss of motor axons progresses between p47 and p90 (Fischer et al., 2004). These pathologies all precede the earliest age of reported motoneuron loss, p80 (Chiu et al., 1995; Fischer et al., 2004), suggesting motoneuron death may be a secondary consequence of primary injuries at the neuromuscular junction (Dupuis et al., 2000). Specifically, loss of contact

between axon terminals and muscle targets may deprive motoneurons of neurotrophic factors necessary for survival (Kiernan et al., 2011).

INTRODUCTION

While the loss of motoneurons is an undisputed feature of amyotrophic lateral sclerosis (ALS) and its animal models (SOD1 mutant mice), how the disease affects the size and shape of motoneurons prior to their degeneration is less well understood. In some of the first morphological evaluations of motoneurons in ALS, Kiernan and Hudson (1991; 1993) reported a decrease in number and cross sectional area of motoneurons in both spinal cord and the hypoglossal nucleus of deceased ALS patients. The authors contend that this observation can be explained by a selective loss of large motoneurons, or by a disease-induced shrinking of motoneurons. Similarly, mice with a rapidly progressing variant of the SOD1 mutation show significantly reduced neuronal volume and number in the facial nucleus, and trends towards reduced size and number in the hypoglossal nucleus at end-stage (Nimchinsky et al., 2000).

However, multiple morphological and electrophysiological reports suggest that at early postnatal stages, motoneurons are pathologically enlarged. Reconstructions of lumbar motoneurons at p4-9 in a slow progressing mSOD1 model reveal an overall increase in neuron size in mutant SOD1 mice as compared to their wildtype littermates. Here, the increase is driven by expansion of the dendritic tree; no changes were evident in soma size (Amendola and Durand, 2008). Lumbar motoneurons from p6-10 mSOD1 mice also show a decreased input resistance and increased capacitance, indicative of larger size (Bories et al., 2007).

These two lines of evidence are not necessarily in conflict. Mutated SOD1 protein may instigate excessive motoneuron growth as part of a suite of early postnatal pathological processes. Compensatory mechanisms may prolong the survival of these enlarged neurons, until a point is reached at which compensation is overwhelmed by the disease processes. Evidence suggests that motoneuron death then proceeds in an order from largest to smallest (Frey et al., 2000a; Pun et al., 2006), allowing the survival of only small motoneurons at end-stage. The course of

these progressive changes highlights the importance of evaluating abnormalities at early age points in addition to end-stage.

A number of additional abnormalities in SOD1 mutant mice can be detected before symptom onset, including: increased neuronal excitability, impaired axon transport, alterations in glutamate receptors, deficits in mitochondrial function, protein ubiquitination, and an imbalance in calcium handling (reviewed in Redler and Dokholyan, 2012). Of these, calcium dynamics may provide a window into ALS pathology, as motoneuron populations resistant to the disease show atypically high calcium buffering capacity (Vanselow and Keller, 2000). In motoneurons, calcium enters through either ligand-gated channels or voltage gated channels. The voltage-gated L-type calcium channel ($Ca_v1.3$) is integral to homeostasis as it mediates the Ca-PIC and can also open to admit calcium at rest (Xu and Lipscombe, 2001). Intracellularly, calcium can be buffered by low levels of the calcium binding proteins calbindin and parvalbumin, but is largely taken up by mitochondria (Lautenschläger et al., 2013). As a result, extensive mitochondrial transport to dendritic space is required to maintain calcium homeostasis. Dysfunction at any of these steps results in elevated intracellular calcium, which serves as a trigger for a number of degenerative cascades, including protein aggregation, mitochondrial dysfunction, and induction of pro-apoptotic pathways (reviewed in Choi, 1988).

One of the earliest (p12) detectable changes in SOD1 motoneurons is an increase in the amplitude of the calcium-mediated persistent inward current (CaPIC), that amplifies synaptic inputs, facilitates repetitive firing and may endow motoneurons with bistable firing patterns (Hounsgaard and Mintz, 1988). In the mouse, the Cav1.3 channel mediating this current develops from little expression at birth to full adult expression levels at two weeks of age. The amplitude of the Ca-PIC increases concurrently (Jiang et al., 1999). While both wild-type and mutant SOD1 mice show elevations in Ca-PIC amplitude during postnatal development, the change is significantly more pronounced in motoneurons of the mSOD1 mouse. This is likely

a result of either accelerated neuronal maturation, or overexpression of the Cav1.3 calcium channel that underlies the PIC (Quinlan et al., 2011).

Interestingly, the early postnatal enlargement of motoneuron size and the increase in Ca-PIC may in fact be linked. As the disease induces a pathological enlargement in motoneuron size, excitability should decrease according to Ohm's law. To preclude reduced excitability, however, neurons may upregulate expression of the Cav1.3 channel responsible for mediating the Ca-PIC, a current integral in establishing the excitability of motoneurons (Hounsgaard and Mintz, 1988).

Some evidence exists to support this hypothesis. Quinlan *et al*.(2011) reported two concurrent alterations in early postnatal SOD1 motoneuron properties: input conductance increases, tending to decrease excitability, but the amplitude of PICs increases, tending to elevate excitability. As a result, net excitability remains unaltered. These findings suggest motoneurons may utilize Ca-PIC enhancement as a compensatory mechanism to maintain excitability despite size increases.

To explore whether there is indeed a correlation between increases in motoneuron size and the upregulation of Cav1.3 channel expression, the present study employed a mutant G93A SOD1 mouse, the most widely used animal model for ALS. This mouse model expresses a human mutant version of the SOD1 gene with a glycine to alanine substitution at position 93, and develops pathology closely mimicking ALS in humans. Clinical disease onset is marked at 90 days, and by the time mice reach end-stage at p136, spinal motoneuron pools show losses of nearly 50% (Chiu et al., 1995). To evaluate changes in size and calcium channel expression in the presymptomatic stage, mice in this study were evaluated at p30, at which point motoneurons do not yet show overt degeneration (Hegedus et al., 2007), but do show alterations in input conductance (Elbasiouny et al., 2010), dendritic outgrowth (Amendola and Durand, 2008), and PIC (van Zundert et al., 2008). A transgenic mouse expressing the wild-type variant of the SOD1 gene was used as a

control group to account for any possible alterations brought on by transfection of human genes (Tortarolo et al., 2004).

In order to compare the effects of the SOD1 mutation on vulnerable and resistant motoneuron populations, this study evaluated changes in motoneurons of the hypoglossal nucleus and cervical and lumbar spinal cord, populations vulnerable to ALS (Gurney et al., 1994b), as well as motoneurons of the oculomotor nucleus, which is known to be remarkably resistant to the disease (Nimchinsky et al., 2000; Haenggeli and Kato, 2002). All three populations show extensive expression of the Cav1.3 channel (Sukiasyan et al., 2009), allowing for an analysis of how the SOD1 mutation may differentially affect expression in the three motoneuron groups.

We anticipated that staining for the Cav1.3 channel would be denser in motoneurons of SOD1 mice, particularly in the vulnerable hypoglossal and spinal populations. Given that Ca-PIC amplitude is increased by p12 in this model, it was reasonable to expect a notable increase in channel expression at p30. In addition, this study tested the hypothesis that an increase in expression levels of the channel giving rise to the Ca-PIC is a compensatory reaction to increased motoneuron size. Accordingly, it was expected that vulnerable motoneurons would be larger in the mutant SOD1 mouse. We were also interested in the confound of sex on the different motoneuron pools as there are several reports indicated that male humans and male mutant mice are more susceptible to the disease progression than females (Veldink et al., 2003; Suzuki et al., 2007; McCombe and Henderson, 2010).

We found no detectable difference between soma area of motoneurons from mice transfected with the ALS mutant gene and its wild-type counterpart. Expression levels of the Cav1.3 calcium channel presented difficulties in analysis across image collection dates, but were not found to be differentiated by genotype, sex, or any interaction of the two. Interestingly, while analysis did not reveal an overall effect of sex on soma size, it did show an interaction effect between the male

sex and SODG93A genotype, leading to a greater increase in soma area in males than in females.

METHODS

Materials. Avidin, biotin, and biotinylated goat anti-rabbit IgG were purchased from Vector (Burlingame, CA). Streptavidin 555 was purchased from Invitrogen (Life Technologies, Grand Island, NY).

Antibodies (anti-CND1) that specifically recognize the α1 subunits of class D ($Ca_V1.3$) Ca^{2+} channels were used in this study. Their generation, purification, and characterization have been reported previously (Hell et al., 1993). Briefly, the CND1 peptide (KYDNKVTIDDYQEEAEDKD; residues 809 to 825, Hui et al., 1991) corresponds to highly variable sites within the intracellular loops between domain II and III of class D α1 subunits of rat brain calcium channels. The NH2-terminal lysine and tyrosine were added for cross-linking and labeling purposes and are not part of the channel sequences. Peptides were synthesized by the solid phase method (Merrifield, 1963), purified by reverse-phase HPLC on a Vydac 218 TP10 column, and confirmed by amino acid analysis. The purified peptides were coupled with glutaraldehyde to bovine serum albumin (Orth, 1979), dialyzed against PBS, and emulsified in the same volume of Freund's complete (initial injection) or incomplete adjuvant. Injections were done in multiple subcutaneous sites on New Zealand white rabbits at three week intervals. Antisera were collected, and antibodies were purified by affinity chromatography on CND1 peptides coupled to CNBr-activated Sepharose. 2 ml of antiserum were adsorbed to the column matrix and incubated at room temperature for 5 h with stirring on a tilting mixer. The columns were then washed with TBS, and bound IgG was eluted with 0.1M glycine (pH 2.7). The affinity-purified anti-CND1 was brought to neutral pH using 0.1M Tris. (Hell et al., 1993)

Animals. Perfused brain tissue of transgenic mice overexpressing the human $SOD1^{G93A}$ gene, the human $SOD1^{WT}$ gene, no transgenic manipulation, and/or

expressing GFP driven by the Hb9 promotor were provided by CJ Heckman's laboratory at Northwestern University. All animals were p29-31 and of mixed sex. In total, data were collected from 25 mice: 9 nontransgenic (5 female, 4 male), 8 WT-SOD1 (4 female, 4 male) and 8 G93A-SOD1 (4 female, 4 male). Tissue was coded prior to shipment to ensure an unbiased, blinded analysis by the University of Washington group. The G93A and wild-type SOD1 genes were identified using standard PCR techniques (Rosen et al., 1993). Briefly, 20-25 mg of tissue was used for the DNA extraction. The primers for amplification are $SOD1^{WT}$: CAT CAG CCC TAA TCC ATC TGA and $SOD1^{G93A}$: CGC GAC TAA CAA TCA AAG TGA, and Hb9:eGFP:AAG TTC ATC TGC ACC ACC G. All mice were used according to Northwestern University's Animal Care and Use Committee guidelines.

Surgery. Mice were euthanized with $C0_2$, and trans-cardially perfused with 4% paraformaldehyde in phosphate buffer (PB). The central nervous system was carefully dissected out and submerged in tubes of 4% paraformaldehyde in PB for 2 hrs at 4°C. The tissue was then cryoprotected by sinking them in 10% sucrose in PB and then in 30% sucrose in PB at 4°C until it was processed for histology.

Immunocytochemistry. Tissue sections (40 μm) were cut on a sliding microtome, placed in 0.1 M phosphate buffer, and then processed for immunocytochemistry as described previously (Westenbroek et al., 1998). Briefly, tissue sections were rinsed in 0.1 M Tris buffer (TB) pH 7.4 for 15 min, in 0.1 M Tris buffered saline (TBS) for 15 min, blocked using 2% avidin in TBS for 30 min., rinsed in TBS for 30 min., blocked in 2% biotin in TBS for 30 min., and finally rinsed in 0.1M TBS for 30 minutes. The tissue sections were then incubated in affinity-purified anti-CND1 (diluted 1:50) for 36 hours at 4°C. All antibodies were diluted in a solution containing 0.1% Triton X-100 and 1% NGS in 0.1M TBS. The tissue sections were rinsed in TBS for 60 min and incubated in biotinylated goat anti-rabbit IgG diluted 1:300 for 1 hr at 37°C. The tissue was then rinsed in TBS for 30 min, incubated in Streptavidin 555 diluted 1:750 for 1 hr at 37°C, then rinsed with TBS for 10 min., rinsed with TB for 20 min

and mounted on charged microscope slides (Fisherbrand Superfrost/Plus), and coverslipped with AquaMount (Fisher).

Image Acquisition and Analysis. Gain- and offset-matched images were collected on a Leica SL confocal microscope in the W.M. Keck Microscopy Facility at the University of Washington. All z-stacks were collected in 1 μm thick sections. To determine the level of nonspecific staining, sections were incubated without primary antibody and the immunocytochemical reaction was then carried out as described above. Sections stained in the absence of primary antibody showed no detectable labeling. A threshold function was applied to all z-stack images, which were custom traced using a Bamboo Create digitizing tablet interfaced with Image J. Motoneuron size and staining density measurements were taken using the Region of Interest (ROI) function in Fiji Image J, which compiled traced outlines of the neuron soma. Each soma was measured for cross sectional area, mean stain intensity (8-bit, max intensity), and roundness, a measure of circularity ranging from 0 to 1 (perfect circle). Roundness measurements were generated using the fit ellipse function on Image J and selecting "shape descriptors" in the measurement options panel.

Neuron selection. In the spinal cord, slices were obtained from all available cervical and lumbar sections. Prominent neurons in the lateral ventral horn were selected and traced for each of the spinal cord sections. The hypoglossal nucleus was clearly delineated by the Cav1.3 stain, and all visible neurons were selected within the boundaries of the nucleus. The oculomotor nucleus was identified with the aid of a comparative Nissl/Cav1.3 staining atlas, and all neurons within boundaries of the nucleus were selected for analysis. Following established guidelines, for all nuclei a subset of the neurons traced were selected as motoneurons based on a threshold of diameter >= 20 um (Rothstein, 1993; Sukiyasan, 2009).

Statistical Analysis

Data regarding cross sectional soma area, roundness, and stain intensity were first pooled across the three genotype groups (nontransgenic, WT-SOD1, G93A-SOD1)

using a one way ANOVA test for significance. However, the ANOVA model does not take into account the correlation that occurs in observations from the same mouse. Observations from the same mouse cannot be treated as independent, as there may be underlying characteristics not captured in the ANOVA model that contribute to similarities within a single mouse.

To remedy this concern about statistical validity, consultation was sought from the statistics graduate program at the University of Washington. Under the guidance of an advisory group (Rachael Maltiel, Bailey Fosdick, Brittany Sanchez, and Dr. Paul Sampson), a mixed linear effects model was developed to account for both fixed effects as well as random effects, which are included to account for variability that may confound the analysis (Kutner et al., 2003). For the purposes of this statistical model, the three genotype groups were narrowed down to the two of interest: the mutant G93A group and the WT-SOD1 group, which serves as a control.

For an example of how the linear mixed effects model generates expected soma cross sectional area, let $Area_{ij}$ be the size of the *jth* observation from mouse *i*. All the explanatory variables are categorical 0-1 indicators of nucleus region, genotype, and sex that a particular observation $Area_{ij}$ pertains to. The reference categories are: oculomotor (nucleus region), WT-SOD (genotype), and female (sex), meaning that the intercept term β_0 is the fitted average area of an oculomotor neuron from a WT-SOD female. The model is expressed:

$$\begin{aligned} Area_{ij} = {} & \beta_0 + \beta_1 \times G93A_i + \beta_2 \times Hypoglossal_{ij} + \beta_3 \times Spinal_{ij} + \beta_4 \times Male_i \\ & + \beta_5 \times Hypoglossal_{ij} \times G93A_i + \beta_6 \times Spinal_{ij} \times G93A_i \\ & + \beta_7 \times G93A_i \times Male_i + \beta_8 \times Hypoglossal_{ij} \times Male_i \\ & + \beta_9 \times Spinal_{ij} \times Male_i + a_i + b_i \times Hypoglossal_{ij} + c_i \times Spinal_{ij} \\ & + \epsilon_{ij} \end{aligned}$$

$$\begin{bmatrix} a_i \\ b_i \\ c_i \end{bmatrix} \sim N(0, \Sigma),$$

$$\epsilon_{ij} \sim N(0, \sigma_\epsilon)$$

The model also includes a random effect a_i for mouse I, capturing mouse to mouse variability for the reference region group. The random slope effects b_i, c_i capture mouse-to-mouse variability of differences from oculomotor to hypoglossal and from oculomotor to spinal. ε_{ij} represents the variability evident within a single mouse and region across multiple observations.

A custom R script was used to generate fitted model coefficients and their corresponding significance values for each of the fixed and random effects, for the parameters of area, roundness, and stain. For the area analysis, the model given above was transformed with a natural logarithmic function to generate more evenly distributed residuals in a QQ plot assessing normality of errors. No transformation was necessary in assessing roundness and stain intensity.

RESULTS

The immunocytochemical staining for Cav1.3 revealed broad and intense expression of the channel throughout the oculomotor, hypoglossal, and spinal nuclei (Fig. 1). Expression levels are so consistently high that the Cav1.3 stain can be used not only to measure channel density, but also to serve as a neuronal marker allowing for measurements of soma size and shape. Confocal images taken with a higher magnification (20x) show that the stain is clear and bright throughout nuclei, with no obvious qualitative differences in Cav1.3 expression levels or soma size between WTSOD and SODG93A mice, in any of the three regions analyzed (Fig. 2).

We measured the soma sizes of spinal (n= 1738; from 19 animals), oculomotor (n= 1140; from 15 animals) and hypoglossal motoneurons (n= 6596 ; from 25 animals) and analyzed the data using a standard one-way ANOVA. The ANOVA revealed small, but statistically significant differences between the three genotype groups (SODG93A, WTSOD, and nontransgenic) for all three nuclei regions, whose density distributions are shown in Figure 3. However, the order of the size differences failed to show a consistent pattern.

In the oculomotor nucleus, motoneurons of WTSOD mice (mean = 260 um^2, SD = 83; 358 motoneurons from 5 animals) and SODG93A mice (mean = 259 um^2, SD = 67; 524 motoneurons from 7 animals) were indistinguishable, while nontransgenic mice had smaller motoneurons (mean = 244 um^2, SD = 63; 258 motoneurons from 3 animals). A one way ANOVA revealed significant differences between the groups ($p = .015$), and Tukey post-hoc tests showed that the SODG93A and WTSOD groups were significantly larger than the nontransgenic group ($p = 0.04$ and 0.02, respectively), but not different from each other.

In the hypoglossal nucleus, motoneurons of nontransgenic mice were the largest (m = 378 um^2, SD = 129; 3239 motoneurons from 9 animals), followed by WTSOD (m = 345 um^2, SD = 127; 1899 motoneurons from 8 animals), with SODG93A motoneurons (m = 320 um^2, SD = 117; 1458 motoneurons from 8

animals) showing the smallest average area ($p<<0.001$ in a one way ANOVA). Post-hoc Tukey tests yielded significant differences in each group comparison ($p <<0.001$ for each comparison).

Data from spinal motoneurons provide an additional inconsistency. Motoneurons of SODG93A mice were the largest (m = 489 um^2, SD = 211; 360 motoneurons from 5 animals), followed by nontransgenic motoneurons (m = 471 um^2, SD = 179; 701 motoneurons from 6 animals), and by motoneurons of WTSOD mice (m = 458 um^2, SD = 178; 677 motoneurons from 8 animals). A one way ANOVA showed the difference in group means to be significant ($p = .03$), and Tukey post-hoc tests showed that this difference stems from the comparison between the WTSOD and SODG93A groups ($p = .03$); all other comparisons were nonsignificant.

The use of a one-way ANOVA presents a number of problems for the present analyses. Ideally, statistical analyses should parse out effects generated by genotype, sex, and region analyzed, as well as interactions between each of those factors. Thus, expanding the model to a two-way ANOVA would still be ineffective in analyzing three converging factors. More importantly, the ANOVA fails to account for individual differences within genotype groups. A valid statistical model cannot treat different observations from the same mouse as independent, as individual variation may confound the analysis. Indeed, Figure 4 shows that average observed soma cross sectional area varies by mouse. As a consequence, motoneuron measurements from different animals in our study cannot be pooled.

To capture individual variability, and also to incorporate data from all animal groups and regions analyzed, a linear mixed effects model was employed as described in the Methods section. As the model is best suited to a comparison of two groups, the analysis focused on mice of SODG3A and WTSOD genotype. WTSOD mice serve as a more rigorous control group than the nontransgenic mice, as simply transfecting mice with a human gene, whether or not that gene predisposes the animal to disease, may alter morphology and physiology (Tortarolo et al., 2004).

With individual differences taken into account, the present sample sizes drop substantially (Table 1). When each neuron was counted as a sampling unit, total sample size exceeded 5,000. When observations from a single mouse were pooled together, the sample size totaled just 16, split evenly among the sex and genotype combination groups. This results in a sizable decrease in statistical power, but does lend greater validity to the analysis.

Fitted average soma cross sectional areas, as calculated by the mixed effects model, are shown in Figure 5, with corresponding coefficients and statistical results listed in Table 2. Overall, there was no effect of genotype (SODG93A vs WTSOD) when other factors (sex and region analyzed) were held constant. Nor was there an effect of sex when genotype and region were held constant. However, the model did reveal an interaction effect between the hypoglossal region and male sex, leading to significantly smaller soma areas for those motoneurons. Also significant was the size order, from spinal motoneurons (largest) to hypoglossal to oculomotor (smallest), all other factors held constant. Perhaps the most intriguing finding was the notable trend toward an interaction effect between the SODG93A genotype and male sex ($p = 0.06$). Here, the mutant genotype displayed a greater increase in soma area in males than in females, within a given region.

To analyze motoneuron shape in addition to size, roundness values were calculated for each motoneuron based on the ratio between the major and minor diameters of a best-fit ellipse (Bernard et al., 2012). The model did not reveal any overall difference in motoneuron roundness by genotype or by sex (Fig. 6). All other factors fixed, spinal motoneurons are significantly rounder ($p < 0.05$), and an interaction effect between the hypoglossal region and the male sex led to significantly less round motoneurons ($p < 0.05$).

Analyzing the intensity of the stain for the calcium channel Cav1.3 presented additional complications. Because the strength of the confocal laser can vary by day, the model was adjusted to include an effect for imaging date. Including this random effect removed the variability associated with changes in the confocal laser, but did

make differences more difficult to parse out. Overall, staining for Cav1.3 is brighter in the spinal motoneurons and does not appear to show any other consistent pattern (Fig. 7). The model did not detect any differences due to genotype, sex, or any interaction therein, but did confirm brighter staining in the spinal cord than in the hypoglossal or oculomotor nuclei ($p < 0.01$).

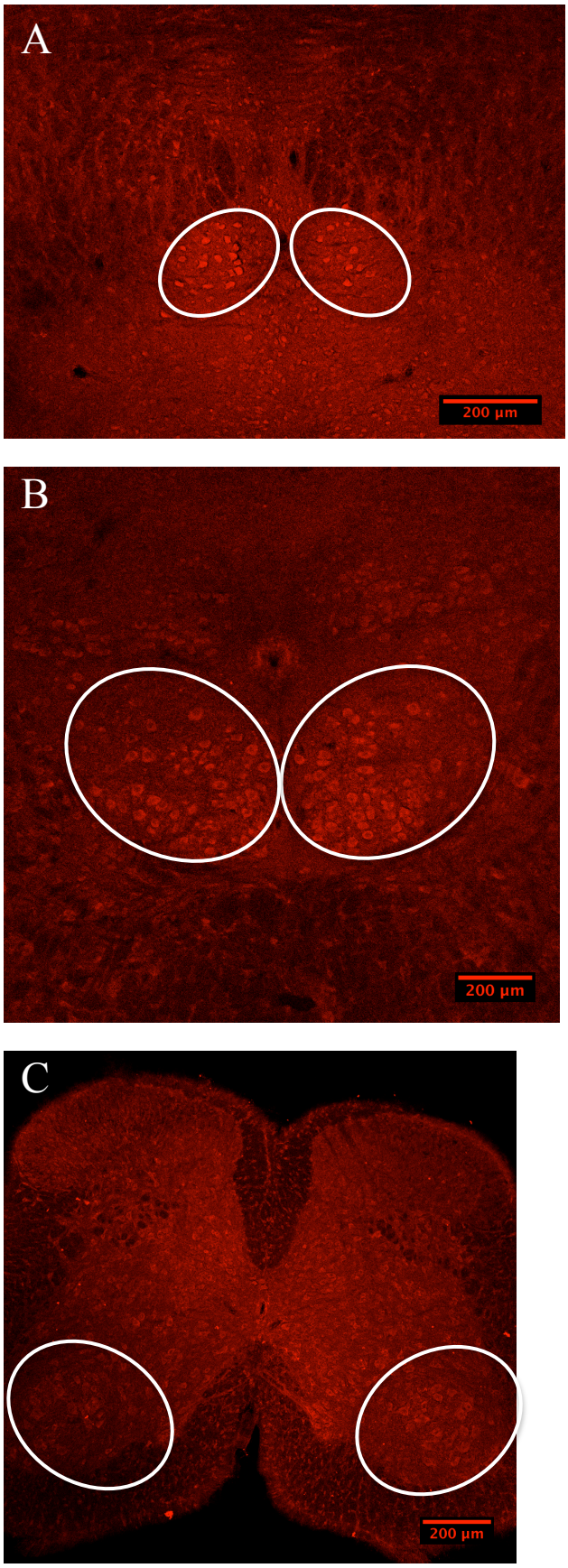

Figure 1. Representative confocal images of Cav1.3 staining in the oculomotor (A), hypoglossal (B) and spinal (C) nuclei. Oval traces indicate region boundaries used for selecting motoneurons. Staining for Cav1.3 is intense and widespread, but particularly concentrated in the large somata of motoneurons.

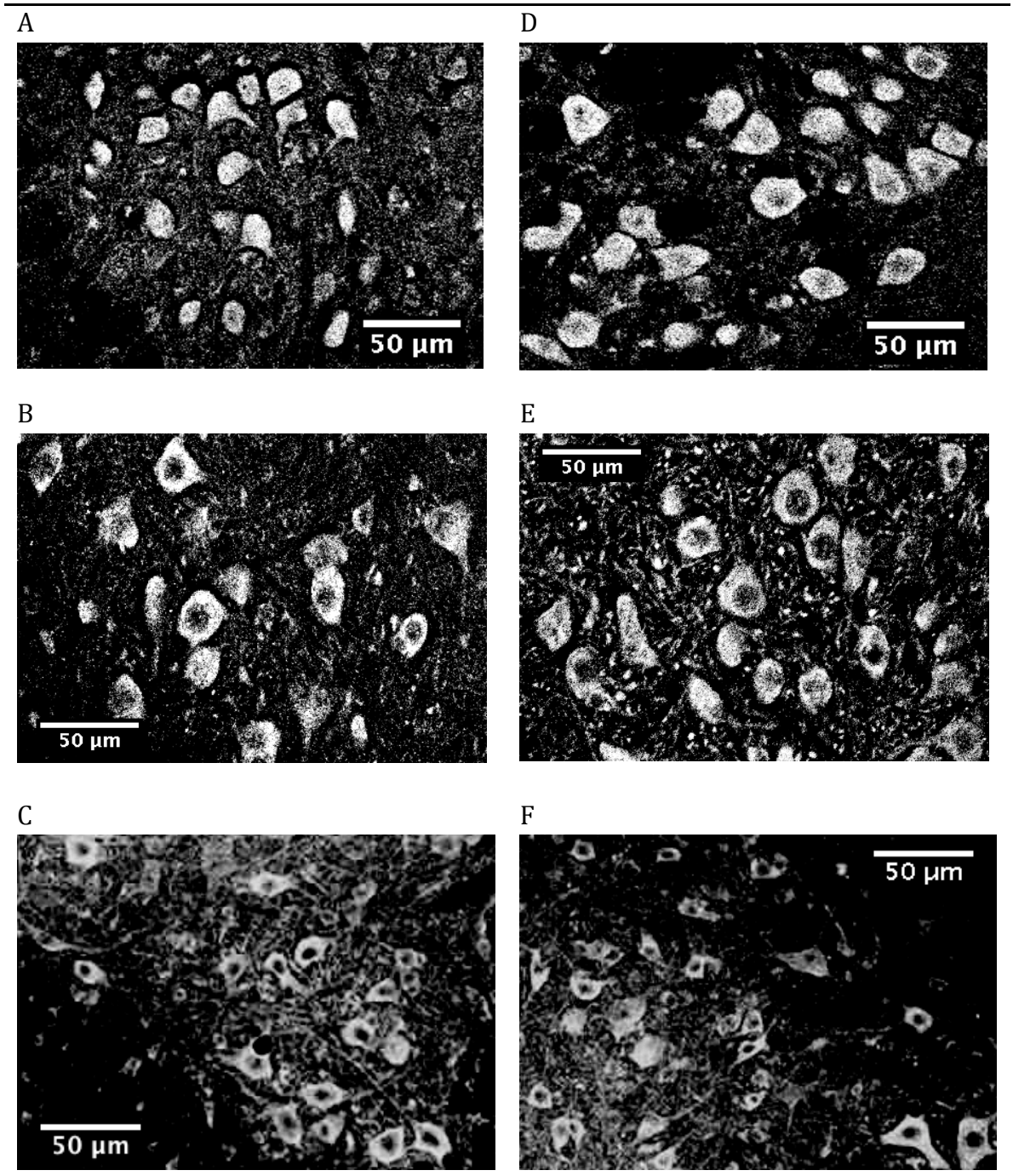

Figure 2. Representative confocal images of Cav1.3 staining in WTSOD (A – C) and SODG93A (D – F) mice in the oculomotor nucleus (A and D), hypoglossal nucleus (B and E) and spinal cord (C and F). Images were acquired through a 20x lens, and threshold-adjusted on black and white spectrum on Image J for optimal

visualization of soma size and shape. Cav1.3 staining is intense throughout the soma in all regions and genotypes analyzed.

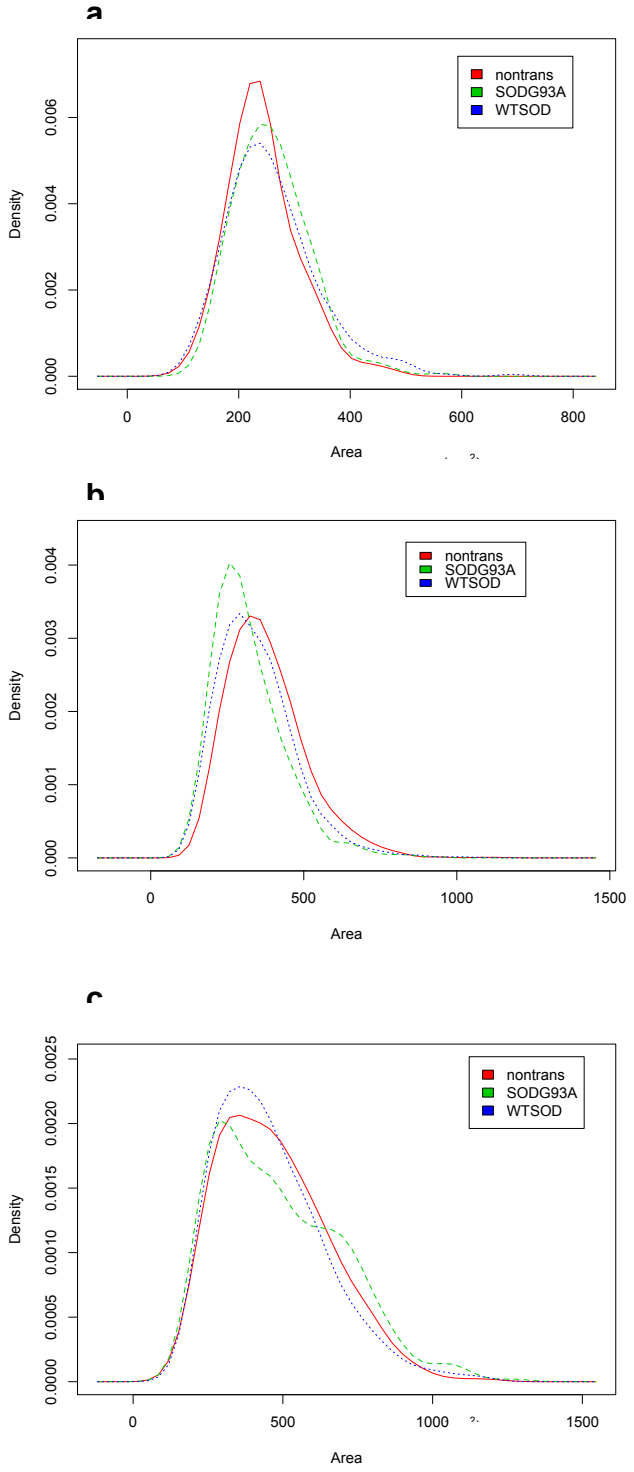

Figure 3. Density plots of somatic size of motoneurons in oculomotor (**a**), hypoglossal (**b**), and spinal (**c**) nuclei sorted by genotype: nontransgenic, SODG93A, and WTSOD. Due to the statistical power afforded by an ANOVA with large sample sizes (> 2,000 neurons per group), small but statistically significant differences were revealed between groups for all three nuclei regions. However, the order of the size differences failed to show a consistent pattern across the three regions.

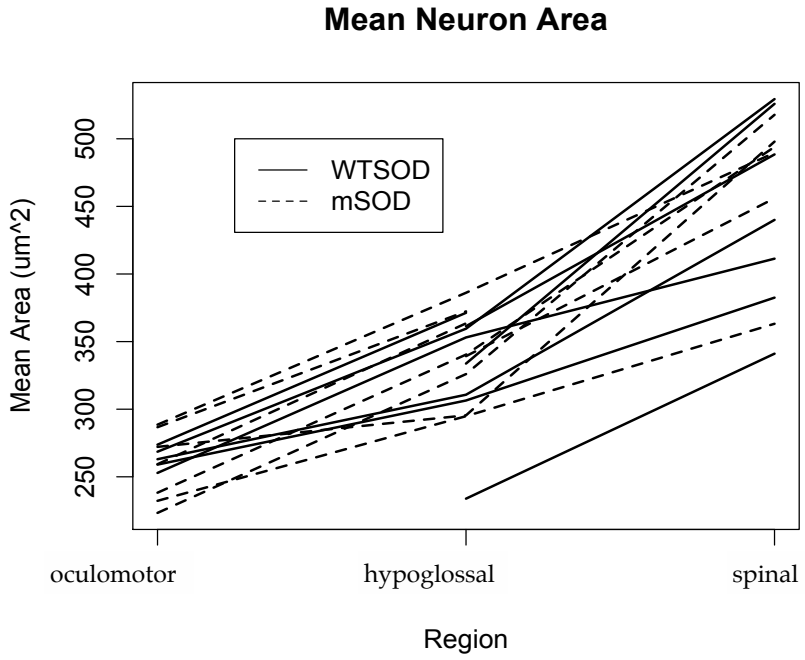

Figure 4. Average observed soma cross sectional area by region across mice distinguished by genotype group (wild-type SOD and mutant G93A SOD). Lines connect the average areas across regions in a single mouse to show individual differences in addition to regional and genotypic differences. Soma sizes are generally largest for spinal motoneurons, followed by motoneurons of the hypoglossal nucleus, and smallest for oculomotor neurons. Appreciable variation is evident between individual mice. Also of note, there does not appear to be a clear distinction between soma sizes pertaining to mice of wild-type versus mutant SOD genotype.

	N, neurons	N, animals
Male, SODG93A	1,112	4
Female, SODG93A	1,230	4
Male, WTSOD	1,292	4
Female, WTSOD	1,642	4
Total	**5,276**	**16**

Table 1. Sample sizes for sex and genotype groupings counted by number of neurons traced (total = 5,276) and by number of animals evaluated per grouping (total = 16). When each neuron is counted as a single observation, the sample sizes in each group are quite large. However, when data are collapsed across animals to account for individual differences, the sample size is reduced substantially. Using the number of animals as a sample size rather than the number of neurons reduces the statistical power but gives greater statistical validity to the analysis.

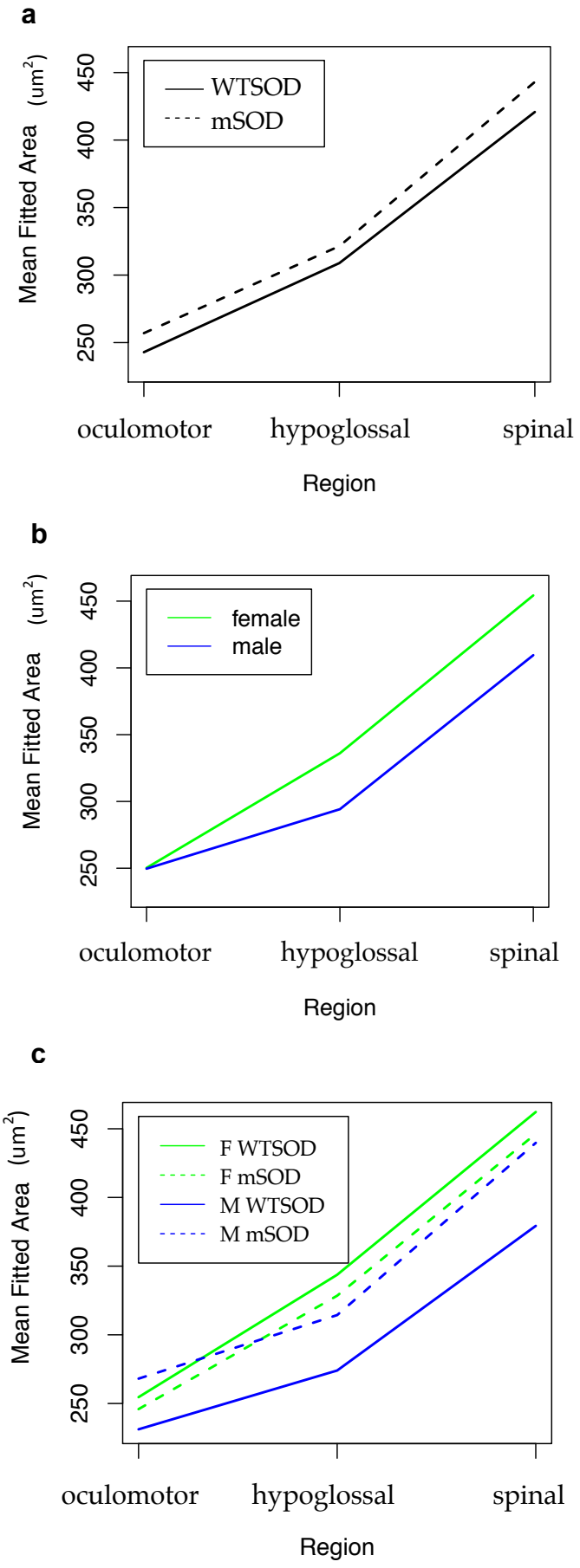

Figure 5. Fitted average soma cross sectional area for oculomotor, hypoglossal, and spinal motoneurons when collapsed across sex to give comparison by genotype (**a**), collapsed across genotype to give comparison by sex (**b**), and separated by sex and genotype to show group specific trends (**c**). Fitted average areas were calculated according to the mixed linear effects model, which was also used to calculate effect size and statistical significance of variable coefficients pertaining to genotype, sex, and region. Though it appears in (**a**) that soma sizes are slightly larger in mutant SOD than wild-type SOD for all regions, the model did not find this difference to be significant. Nor did the model find an overall sex difference in soma area, though as evident in (**b**), there is an interaction effect between the hypoglossal region and male sex, leading to significantly smaller fitted area. A nonparallel relationship between mutant and wild-type status for females and males is evident in (**c**), indicating that the mutant genotype and male sex interact to enlarge soma area (see Table 2 for model coefficients and statistical significance).

	Estimate	p-value
β_0 = Intercept	**5.54**	**<0.001**
β_1 = SODG93A	-0.03	0.583
β_2 = Hypoglossal	**0.30**	**<0.001**
β_3 = Spinal	**0.60**	**<0.001**
β_4 = Male	-0.10	0.17
β_5 = Hypoglossal x SODG93A	-0.01	0.752
β_6 = Spinal x SODG93A	0	0.997
β_7 = SODG93A x Male	0.18	0.062
β_8 = Hypoglossal x Male	**-0.13**	**0.002**
β_9 = Spinal x Male	-0.10	0.136

Table 2: Fitted model coefficients for linear mixed effects model giving soma area. The model uses a reference group of oculomotor neurons from a WTSOD female; all values listed here are generated in comparison to this reference group. For soma area, the model was log transformed to normalize residuals. All significant coefficients are in bold and include: intercept (as expected; a nonsignificant intercept would indicate that the mean log area of the reference group is 0), hypoglossal and spinal groups (indicating greater soma area in these groups than the reference oculomotor group), and an interaction between the hypoglossal group and male sex (indicating a nonparallel relationship between mutant SOD status and sex).

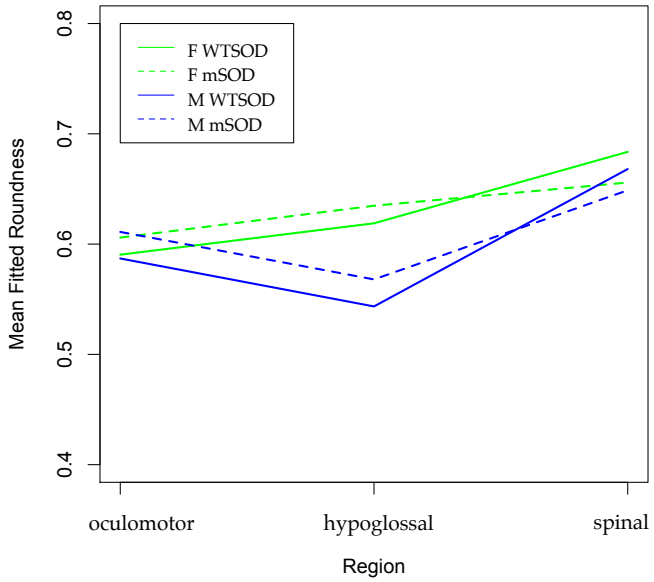

Figure 6. Mean fitted roundness values for oculomotor, hypoglossal, and spinal motoneurons grouped by sex and genotype. Roundness was determined by the ratio of major diameter to minor diameter in a best fit ellipse generated by ImageJ, and ranges from 0 to 1 (perfect circle). There are no overall statistically significant differences in roundness between genotypes or sexes, though the model does reveal rounder motoneurons in the spinal cord, and an interaction effect between the hypoglossal region and the male sex leading to less round motoneurons.

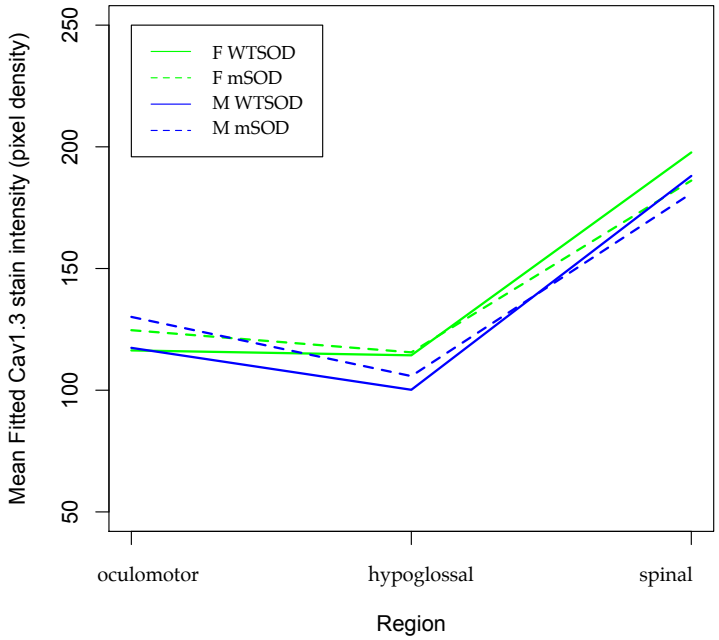

Figure 7. Mean fitted Cav1.3 stain intensity for oculomotor, hypoglossal, and spinal motoneurons grouped by sex and genotype. Stain intensity was measured by the average pixel density of grouped z-stacks in ImageJ, and ranges from 0 – 256. The model used to analyze stain density incorporated an additional random effect for date of image acquisition, as laser intensity on the confocal microscope can vary day to day. There are no overall statistically significant differences in Cav1.3 staining intensity between genotypes or sexes. The model did confirm more intense staining in motoneurons of the spinal cord than of the hypoglossal or oculomotor nuclei.

DISCUSSION

This study tested the hypothesis that motoneurons in mutant SODG93A mice exhibit an enlargement of soma size (i.e., cross-sectional area) and an increase in Cav1.3 channel expression at p30, well before the manifestation of physiological symptoms, which typically occur at p90 (Chiu et al., 1995). We made measurements of spinal and hypoglossal motoneurons vulnerable to the mutation, as well as motoneurons in the oculomotor nucleus that are resistant. We did not find any significant differences in soma size for mutant and wild-type motoneurons in any of the motor nuclei. Nor did our analyses reveal any difference in shape, measured as the roundness of the soma. Similarly, levels of the Cav1.3 calcium channel were not found to be differentiated by genotype, sex or any interaction of the two.

These results find mixed support in a conflicting body of literature regarding the effects of the SOD1 mutation on early postnatal motoneuron size. A number of studies report an increase in total input conductance, an electrical measurement indicative of larger neuronal size, in early postnatal SOD1 motoneurons (Bories et al., 2007; Elbasiouny et al., 2010; Quinlan et al., 2011), though no difference was reported in p4-10 hypoglossal motoneurons (van Zundert et al., 2008). However, morphological analyses show no difference in soma size between mutant and WT SOD motoneurons (Kuo et al., 2004; Amendola and Durand, 2008).

The most parsimonious explanation for these seemingly disparate results may be that motoneuron enlargement is rooted in an expansion of the dendritic tree, which will affect physiological measurements, and can occur independently of any increase in soma size (Amendola and Durand, 2008). Indeed, Amendola and Durand (2008) report a proliferation of distal dendritic branches in lumbar motoneurons of young SOD1 mice, without any change in soma size, number, or mean diameter of primary dendrites. The present study, which was limited to somatic dimensions as a metric for motoneuron size, may have failed to capture real differences that exist between the mutant and wild-type animals.

The one striking difference we did observe was an interaction effect between sex and SODG93A genotype: namely that the motoneurons in mutant males are significantly larger than those in mutant females. This finding raises two questions: does the incidence and course of ALS-like symptoms is SOD1 mice differ between males and females? And further, how might the mutant SOD1 protein interact differently with motoneurons by sex?

A recent literature review of sex differences in ALS concluded that the incidence and prevalence of ALS are greater in men than in women. However, this sex difference is found only in large studies including both sporadic and familial ALS cases, and disappears when familial ALS is studied independently (McCombe and Henderson, 2010). Given that the SOD1 mouse is thought to model the familial form of the disease, it is logical to question whether the animal model adequately captures the sex differences found in the sporadic form, which accounts for 90 – 95% of cases. In fact, SOD1 mutant mice do show earlier disease onset in males than in females (Veldink et al., 2003; Suzuki et al., 2007), though no effect of sex on loss of muscle force is evident (Hegedus et al., 2009).

What is it about being male that might accelerate the onset of the disease, and can the root be traced to differences in the physiology of motoneurons? Sex differences in disease course typically raise the possibility of the involvement of sex steroid hormones in etiopathogenesis. In ALS, there is limited but intriguing evidence for hormone involvement. The male sex is associated with higher levels of prenatal testosterone (Slob et al., 1980). However, a recent examination of finger length ratios, a surrogate marker for prenatal testosterone levels, revealed that both men and women with ALS were exposed to higher prenatal testosterone than were healthy controls (Vivekananda et al., 2011).

In embryonic cultures, motoneurons transfected with human androgen receptors exhibit a dose-dependent change in morphology in response to androgen treatment, developing larger cell bodies and broader dendritic processes (Brooks et al., 1998). Thus, elevated prenatal testosterone levels may predispose motoneurons

to abnormal growth. Further, this predisposition may be more likely to actualize in males, whose naturally higher testosterone levels may be more precariously balanced between its beneficial effects on motoneuron survival (Jones, 1994), and induction of excessive growth (Brooks et al., 1998).

Very little is known about whether sex steroid hormones may also influence expression levels of the Cav1.3 calcium channel. In the only known study of this possible relationship, Cav1.3 mRNA levels were found to be higher in male wild type mice than in females (Li et al., 2010). The present data did not uncover any sex differences in expression levels of Cav1.3. Nor were any differences detected between mutant and wild-type SOD1 genotypes. These result appears to stand in contrast with a report of greater Ca-PIC amplitude in juvenile mutant SOD1 mice (Quinlan et al., 2011).

There are two possible explanations that may reconcile the enhanced Ca-PIC amplitude in mutant SOD1 mice mentioned above (Quinlan et al., 2011) with the absence of an evident change in somatic expression of the Cav1.3 channel responsible for that current reported here. First, the Ca-PIC is largely a current of dendritic origin (Lee and Heckman, 1996; Carlin et al., 2000b). The Cav1.3 channel is expressed widely throughout the neuron body and its processes (Sukiasyan et al., 2009), but modulation of its expression may be localized to its more active presence in dendritic processes. Cav1.3 expression may not change at the soma in the SODG93A mouse, but may be upregulated in the dendritic tree, which could not be imaged using the techniques employed in this study.

Alternatively, it is possible that the Ca-PIC is elevated not through an expansion of the number of Cav1.3 channels, but through an increase in the open probability or activation threshold of the existing channel population. Van Zundert *et al.* (2008) reported an increase in early postnatal Na-PIC without a corresponding increase in the density of the responsible channels. The authors suggest that the effect is achieved instead through a premature Na channel isoform turnover to isoforms that permit greater levels of persistent activity. Recently, several splice

variants of the Cav1.3 channel have been identified, composing a range of activation thresholds and open probabilities (Bock et al., 2011). While the effects of the SOD1 mutation on Cav1.3 isoform diversity have yet to be explored, modulation of channel variant presents one possible pathway to overall current enhancement.

A number of procedural choices made in the design of this study may have limited the range of statistical inferences that could be drawn from the data. First, the decision to pool motoneurons by animal lent greater validity to the analysis but somewhat paradoxically drastically reduced its statistical power. We found small, but significant differences in the soma sizes of nearly every animal and thus, each animal yielded but a single datum. As individual variations must be taken into account, a much larger number of animals in each genotype and sex group would be needed to increase statistical power. Some of the trends found here, like the interaction effect between male sex and SODG93A genotype ($p = 0.06$), an interaction effect between male sex and spinal motoneuron size ($p = 0.14$) and an overall effect of male sex ($p = 0.17$) might reach statistical significance with a greater sample size.

Second, technical limitations of Cav1.3 immunocytochemistry and confocal microscopy meant that only the motoneuron somata could be analyzed for channel expression and size. Since both neuron growth (Amendola and Durand, 2008) and Ca-PIC (Carlin et al., 2000b) have been shown to be highly concentrated in the dendritic regions, future studies should employ techniques that allow for data acquisition from the dendritic tree. Finally, future studies should examine mutant SOD1 effects at a range of age points. The timeline of ALS pathology has proved difficult to parse out; a better understanding of temporal relationships between pathological events will help distinguish between primary and compensatory mechanisms (Quinlan, 2011).

REFERENCES

Alexianu ME, Ho BK, Mohamed AH, La Bella V, Smith RG, Appel SH (1994) The role of calcium-binding proteins in selective motoneuron vulnerability in amyotrophic lateral sclerosis. Ann Neurol 36:846–858.

Amendola J, Durand J (2008) Morphological differences between wild-type and transgenic superoxide dismutase 1 lumbar motoneurons in postnatal mice. J Comp Neurol 511:329–341.

Angenstein F, Niessen HG, Goldschmidt J, Vielhaber S, Ludolph AC, Scheich H (2004) Age-dependent changes in MRI of motor brain stem nuclei in a mouse model of ALS. Neuroreport 15:2271–2274.

Beers DR, Ho BK, Siklos L, Alexianu ME, Mosier DR, Mohamed AH, Otsuka Y, Kozovska ME, McAlhany RE, Smith RG (2001) Parvalbumin overexpression alters immune-mediated increases in intracellular calcium, and delays disease onset in a transgenic model of familial amyotrophic lateral sclerosis. Journal of Neurochemistry 79:499–509.

Bendotti C, Calvaresi N, Chiveri L, Prelle A, Moggio M, Braga M, Silani V, De Biasi S (2001) Early vacuolization and mitochondrial damage in motor neurons of FALS mice are not associated with apoptosis or with changes in cytochrome oxidase histochemical reactivity. J Neurol Sci 191:25–33.

Bensimon G, Lacomblez L (1994) A Controlled Trial of Riluzole in Amyotrophic Lateral Sclerosis. New England Journal of ….

Bernard AB, Lin C-C, Anseth KS (2012) A microwell cell culture platform for the aggregation of pancreatic β-cells. Tissue Eng Part C Methods 18:583–592.

Bernard-Marissal N, Moumen A, Sunyach C, Pellegrino C, Dudley K, Henderson CE, Raoul C, Pettmann B (2012) Reduced calreticulin levels link endoplasmic reticulum stress and Fas-triggered cell death in motoneurons vulnerable to ALS. J Neurosci 32:4901–4912.

Bjornskov EK, Norris FH Jr, Mower-Kuby J (1984) Quantitative axon terminal and end-plate morphology in amyotrophic lateral sclerosis. Archives of Neurology 41:527.

Bock G, Gebhart M, Scharinger A, Jangsangthong W, Busquet P, Poggiani C, Sartori S, Mangoni ME, Sinnegger-Brauns MJ, Herzig S, Striessnig J, Koschak A (2011) Functional properties of a newly identified C-terminal splice variant of Cav1.3 L-type Ca2+ channels. J Biol Chem 286:42736–42748.

Bories C, Amendola J, Lamotte d'Incamps B, Durand J (2007) Early electrophysiological abnormalities in lumbar motoneurons in a transgenic mouse model of amyotrophic lateral sclerosis. Eur J Neurosci 25:451–459.

Breuer AC, Atkinson MB (1988) Calcium dependent modulation of fast axonal transport. Cell Calcium 9:293–301.

Breuer AC, Bond M, Atkinson MB (1992) Fast axonal transport is modulated by altering trans-axolemmal calcium flux. Cell Calcium 13:249–262.

Brooks BP, Merry DE, Paulson HL, Lieberman AP, Kolson DL, Fischbeck KH (1998) A cell culture model for androgen effects in motor neurons. Journal of Neurochemistry 70:1054–1060.

Bruijn LI, Becher MW, Lee MK, Anderson KL, Jenkins NA, Copeland NG, Sisodia SS, Rothstein JD, Borchelt DR, Price DL, Cleveland DW (1997) ALS-linked SOD1 mutant G85R mediates damage to astrocytes and promotes rapidly progressive disease with SOD1-containing inclusions. Neuron 18:327–338.

Carlin KP, Jiang Z, Brownstone RM (2000a) Characterization of calcium currents in functionally mature mouse spinal motoneurons. Eur J Neurosci 12:1624–1634.

Carlin KP, Jones KE, Jiang Z, Jordan LM, Brownstone RM (2000b) Dendritic L-type calcium currents in mouse spinal motoneurons: implications for bistability. Eur J Neurosci 12:1635–1646.

Carrascal L, Nieto-Gonzalez JL, Cameron WE, Torres B, Nunez-Abades PA (2005) Changes during the postnatal development in physiological and anatomical characteristics of rat motoneurons studied in vitro. Brain Res Brain Res Rev 49:377–387.

Carriedo SG, Sensi SL, Yin HZ, Weiss JH (2000) AMPA Exposures Induce Mitochondrial Ca2+ Overload and ROS Generation in Spinal Motor Neurons In Vitro. The Journal of ….

Charcot JM (1874) De la sclérose latérale amyotrophique. Progr Méd(Paris).

Chiu AY, Zhai P, Dal Canto MC, Peters TM, Kwon YW, Prattis SM, Gurney ME (1995) Age-dependent penetrance of disease in a transgenic mouse model of familial amyotrophic lateral sclerosis. Mol Cell Neurosci 6:349–362.

Choi DW (1987) Ionic dependence of glutamate neurotoxicity.

Choi DW (1988) Calcium-mediated neurotoxicity: relationship... [Trends Neurosci. 1988] - PubMed - NCBI. Trends Neurosci.

Cleveland DW, Rothstein JD (2001) From Charcot to Lou Gehrig: deciphering selective motor neuron death in ALS. Nat Rev Neurosci.

Corona JC, Tapia R (2007) Ca2+-permeable AMPA receptors and intracellular Ca2+ determine motoneuron vulnerability in rat spinal cord in vivo. Neuropharmacology 52:1219–1228.

Crapo JD, Oury T, Rabouille C, Slot JW, Chang LY (1992) Copper,zinc superoxide dismutase is primarily a cytosolic protein in human cells. Proc Natl Acad Sci USA 89:10405–10409.

Damiano M, Starkov AA, Petri S, Kipiani K, Kiaei M, Mattiazzi M, Flint Beal M, Manfredi G (2006) Neural mitochondrial Ca2+ capacity impairment precedes the onset of motor symptoms in G93A Cu/Zn-superoxide dismutase mutant mice. Journal of Neurochemistry 96:1349–1361.

De Vos KJ, Chapman AL, Tennant ME, Manser C, Tudor EL, Lau K-F, Brownlees J, Ackerley S, Shaw PJ, McLoughlin DM, Shaw CE, Leigh PN, Miller CCJ, Grierson AJ (2007) Familial amyotrophic lateral sclerosis-linked SOD1 mutants perturb fast axonal transport to reduce axonal mitochondria content. Hum Mol Genet 16:2720–2728.

Dengler R, Konstanzer A, K ther G, Hesse S, Wolf W, Strupplerdr A (1990) Amyotrophic lateral sclerosis: Macro-EMG and twitch forces of single motor units. Muscle Nerve 13:545–550.

DePaul R, Abbs JH, Caligiuri M, Gracco VL, Brooks BR (1988) Hypoglossal, trigeminal, and facial motoneuron involvement in amyotrophic lateral sclerosis. Neurology 38:281–281.

Dubrovsky B, Filipini D (1990) Neurobiological aspects of the pelvic floor muscles involved in defecation. Neuroscience & Biobehavioral Reviews.

Dupuis L, de Tapia M, René F, Lutz-Bucher B, Gordon JW, Mercken L, Pradier L, Loeffler JP (2000) Differential screening of mutated SOD1 transgenic mice reveals early up-regulation of a fast axonal transport component in spinal cord motor neurons. Neurobiol Dis 7:274–285.

Eisen A, Swash M (2001) Clinical neurophysiology of ALS. Clinical Neurophysiology 112:2190–2201.

Elbasiouny SM, Amendola J, Durand J, Heckman CJ (2010) Evidence from computer simulations for alterations in the membrane biophysical properties and dendritic processing of synaptic inputs in mutant superoxide dismutase-1 motoneurons. J Neurosci 30:5544–5558.

Elliott JL, Snider WD (1995) Parvalbumin is a marker of ALS-resistant motor neurons. Neuroreport 6:449–452.

Estevez AG, Stutzmann J-M, Barbeito L (1995) Protective effect of riluzole on excitatory amino acid-mediated neurotoxicity in motoneuron-enriched cultures. European Journal of Pharmacology 280:47–53.

Ferrucci M, Spalloni A, Bartalucci A, Cantafora E, Fulceri F, Nutini M, Longone P, Paparelli A, Fornai F (2010) A systematic study of brainstem motor nuclei in a mouse model of ALS, the effects of lithium. Neurobiol Dis 37:370–383.

Fischer LR, Culver DG, Tennant P, Davis AA, Wang M, Castellano-Sanchez A, Khan J, Polak MA, Glass JD (2004) Amyotrophic lateral sclerosis is a distal axonopathy: evidence in mice and man. Exp Neurol 185:232–240.

Frey D, Schneider C, Xu L, Borg J, Spooren W, Caroni P (2000a) Early and selective loss of neuromuscular synapse subtypes with low sprouting competence in motoneuron diseases. J Neurosci 20:2534–2542.

Frey D, Schneider C, Xu L, Borg J, Spooren W, Caroni P (2000b) Early and Selective Loss of Neuromuscular Synapse Subtypes with Low Sprouting Competence in Motoneuron Diseases. The Journal of ….

Gould TW (2006) Complete Dissociation of Motor Neuron Death from Motor Dysfunction by Bax Deletion in a Mouse Model of ALS. J Neurosci 26:8774–8786.

Gurney ME, Cutting FB, Zhai P, Doble A, Taylor CP, Andrus PK, Hall ED (1996) Benefit of vitamin E, riluzole, and gababapentin in a transgenic model of familial amyotrophic lateral sclerosis. Ann Neurol 39:147–157.

Gurney ME, Pu H, Chiu AY, Dal Canto MC, Polchow CY, Alexander DD, Caliendo J, Hentati A, Kwon YW, Deng H-X (1994a) Motor neuron degeneration in mice that express a human Cu, Zn superoxide dismutase mutation. Science:1772–1772.

Gurney ME, Pu H, Chiu AY, Dal Canto MC, Polchow CY, Alexander DD, Caliendo J, Hentati A, Kwon YW, Deng HX (1994b) Motor neuron degeneration in mice that express a human Cu,Zn superoxide dismutase mutation. Science 264:1772–1775.

Haenggeli C, Kato AC (2002) Differential vulnerability of cranial motoneurons in mouse models with motor neuron degeneration. Neurosci Lett 335:39–43.

Hammerschlag R, Dravid A, Chiu A (1975) Mechanism of axonal transport: a proposed role for calcium ions. Science 188:273–275.

Hanyu N, Oguchi K, Yanagisawa N, Tsukagoshi H (1982) Degeneration and regeneration of ventral root motor fibers in amyotrophic lateral sclerosis. J Neurol Sci 55:99–115.

Hayashi H, Kato S (1989) Total manifestations of amyotrophic lateral sclerosis. ALS in the totally locked-in state. J Neurol Sci 93:19–35.

Heckman CJ, Johnson M, Mottram C, Schuster J (2008) Persistent inward currents in spinal motoneurons and their influence on human motoneuron firing patterns. The Neuroscientist 14:264–275.

Hegedus J, Putman CT, Gordon T (2007) Time course of preferential motor unit loss in the SOD1 G93A mouse model of amyotrophic lateral sclerosis. Neurobiol Dis 28:154–164.

Hegedus J, Putman CT, Gordon T (2009) Progressive motor unit loss in the G93A mouse model of amyotrophic lateral sclerosis is unaffected by gender. Muscle Nerve 39:318–327.

Henneman E (1957) Relation between size of neurons and their susceptibility to discharge. Science 126:1345–1347.

Henneman E, Somjen G, Carpenter DO (1965) Functional significance of cell size in spinal motoneurons. J Neurophysiol 28:560–580.

Hounsgaard J, Kiehn O (1989) Serotonin-induced bistability of turtle motoneurones caused by a nifedipine-sensitive calcium plateau potential. The Journal of Physiology 414:265–282.

Hounsgaard J, Kiehn O (1993) Calcium spikes and calcium plateaux evoked by differential polarization in dendrites of turtle motoneurones in vitro. The Journal of Physiology.

Hounsgaard J, Mintz I (1988) Calcium conductance and firing properties of spinal motoneurones in the turtle. The Journal of Physiology 398:591–603.

Iwata M, Inoue K, Hirano A (1978) Sparing of the Onufrowicz Nucleus in Anterior Horn Diseases. J Neuropathol Exp Neurol 37:636.

Jiang Z, Carlin KP, Brownstone RM (1999a) An in vitro functionally mature mouse spinal cord preparation for the study of spinal motor networks. Brain Res 816:493–499.

Jiang Z, Rempel J, Li J, Sawchuk MA, Carlin KP, Brownstone RM (1999b) Development of L-type calcium channels and a nifedipine-sensitive motor activity in the postnatal mouse spinal cord. Eur J Neurosci 11:3481–3487.

Jones KJ (1994) Androgenic Enhancement of Motor Neuron Regeneration - JONES - 2006 - Annals of the New York Academy of Sciences - Wiley Online Library. Ann N Y Acad Sci.

Kennel PF, Finiels F, Revah F, Mallet J (1996) Neuromuscular function impairment is not caused by motor neurone loss in FALS mice: an electromyographic study. Neuroreport 7:1427–1431.

Kiernan JA, Hudson AJ (1991) Changes in sizes of cortical and lower motor neurons in amyotrophic lateral sclerosis. Brain 114 (Pt 2):843–853.

Kiernan JA, Hudson AJ (1993) Changes in shapes of surviving motor neurons in amyotrophic lateral sclerosis. Brain 116 (Pt 1):203–215.

Kiernan MC, Vucic S, Cheah BC, Turner MR, Eisen A, Hardiman O, Burrell JR, Zoing MC (2011) Amyotrophic lateral sclerosis. Lancet 377:942–955.

Kong J, Xu Z (1998) Massive mitochondrial degeneration in motor neurons triggers the onset of amyotrophic lateral sclerosis in mice expressing a mutant SOD1. J Neurosci 18:3241–3250.

Kuo JJ, Schonewille M, Siddique T, Schults ANA, Fu R, Bär PR, Anelli R, Heckman CJ, Kroese ABA (2004) Hyperexcitability of cultured spinal motoneurons from presymptomatic ALS mice. J Neurophysiol 91:571–575.

Kuo JJ, Siddique T, Fu R, Heckman CJ (2005) Increased persistent Na(+) current and its effect on excitability in motoneurones cultured from mutant SOD1 mice. The Journal of Physiology 563:843–854.

Kurtzke JF (1982) Epidemiology of amyotrophic lateral sclerosis. [Adv Neurol. 1982] - PubMed - NCBI. Adv Neurol.

Kutner MH, Nachtsheim CJ, Neter J (2003) Applied Linear Regression Models. McGraw-Hill/Irwin.

Lacomblez L, Bensimon G, Leigh PN, Guillet P, Meininger V (1996) Dose-ranging study of riluzole in amyotrophic lateral sclerosis. Amyotrophic Lateral Sclerosis/Riluzole Study Group II. Lancet 347:1425–1431.

Larivière L, Lavoie PA (1982) Calcium requirement for fast axonal transport in frog motoneurons. Journal of Neurochemistry 39:882–886.

Lautenschläger J, Prell T, Ruhmer J, Weidemann L, Witte OW, Grosskreutz J (2013) Overexpression of human mutated G93A SOD1 changes dynamics of the ER mitochondria calcium cycle specifically in mouse embryonic motor neurons. Exp Neurol.

Lee RH, Heckman CJ (1996) Influence of voltage-sensitive dendritic conductances on bistable firing and effective synaptic current in cat spinal motoneurons in vivo. J Neurophysiol 76:2107–2110.

Lee RH, Heckman CJ (1999) Paradoxical Effect of QX-314 on Persistent Inward Currents and Bistable Behavior in Spinal Motoneurons In Vivo.

Lewinski von F, Keller BU (2005a) Ca2+, mitochondria and selective motoneuron vulnerability: implications for ALS. Trends Neurosci 28:494–500.

Lewinski von F, Keller BU (2005b) Mitochondrial Ca2+ buffering in hypoglossal motoneurons from mouse. Neurosci Lett 380:203–208.

Li J, Zhao L, Ferries IK, Jiang L, Desta MZ, Yu X, Yang Z, Duncan RL, Turner CH (2010) Skeletal phenotype of mice with a null mutation in Cav 1.3 L-type calcium channel. J Musculoskelet Neuronal Interact 10:180–187.

Li Y, Bennett DJ (2003) Persistent sodium and calcium currents cause plateau potentials in motoneurons of chronic spinal rats. J Neurophysiol 90:857–869.

Li Y, Gorassini MA, Bennett DJ (2004) Role of persistent sodium and calcium currents in motoneuron firing and spasticity in chronic spinal rats. J Neurophysiol 91:767–783.

Lips MB, Keller BU (1998) Endogenous calcium buffering in motoneurones of the nucleus hypoglossus from mouse. The Journal of Physiology 511 (Pt 1):105–117.

Liu C-H, Jiao H, Guo Z-H, Peng Y, Wang W-Z (2013) Up-regulated GLT-1 resists glutamate toxicity and attenuates glutamate-induced calcium loading in cultured neurocytes. Basic Clin Pharmacol Toxicol 112:19–24.

Lledo PM, Somasundaram B, Morton AJ, Emson PC (1992) ScienceDirect.com - Neuron - Stable transfection of calbindin-D28k into the GH3 cell line alters calcium currents and intracellular calcium homeostasis. Neuron.

Martin LJ, Liu Z, Chen K, Price AC, Pan Y, Swaby JA, Golden WC (2006) Motor neuron degeneration in amyotrophic lateral sclerosis mutant superoxide dismutase-1 transgenic mice: Mechanisms of mitochondriopathy and cell death. J Comp Neurol 500:20–46.

Mattson MP, Guthrie PB, Kater SB (1989) A role for Na+-dependent Ca2+ extrusion in protection against neuronal excitotoxicity. FASEB J 3:2519–2526.

McComas AJ, Sica REP, Campbell MJ, Upton ARM (1971) Functional compensation in

partially denervated muscles. J Neurol Neurosurg Psychiatr 34:453–460.

McCombe PA, Henderson RD (2010) Effects of gender in amyotrophic lateral sclerosis. Gend Med 7:557–570.

Meehan CF, Moldovan M, Marklund SL, Graffmo KS, Nielsen JB, Hultborn H (2010) Intrinsic properties of lumbar motor neurones in the adult G127insTGGG superoxide dismutase-1 mutant mouse in vivo: evidence for increased persistent inward currents. Acta Physiol (Oxf) 200:361–376.

Miles GB, Lipski J, Lorier AR, Laslo P, Funk GD (2004) Differential expression of voltage-activated calcium channels in III and XII motoneurones during development in the rat. Eur J Neurosci 20:903–913.

Millecamps S, Nicolle D, Ceballos-Picot I, Mallet J, Barkats M (2001) Synaptic sprouting increases the uptake capacities of motoneurons in amyotrophic lateral sclerosis mice. Proc Natl Acad Sci USA 98:7582–7587.

Miller RJ, Murphy SN, Glaum SR (1989) Neuronal Ca2+ channels and their regulation by excitatory amino acids. Ann N Y Acad Sci 568:149–158.

Mórotz GM, De Vos KJ, Vagnoni A, Ackerley S, Shaw CE, Miller CCJ (2012) Amyotrophic lateral sclerosis-associated mutant VAPBP56S perturbs calcium homeostasis to disrupt axonal transport of mitochondria.

Mulder DW, Howard FM Jr (1976) Patient resistance and prognosis in amyotrophic lateral sclerosis. Mayo Clinic proceedings Mayo Clinic.

Munoz D, Greene C, Perl D, Selkoe D (1988) Accumulation of phosphorylated neurofilaments in anterior horn motoneurons of amyotrophic lateral sclerosis patients. J Neuropathol Exp Neurol 47:9.

Nieto-Gonzalez JL, Moser J, Lauritzen M, Schmitt-John T, Jensen K (2011) Reduced GABAergic inhibition explains cortical hyperexcitability in the wobbler mouse model of ALS. Cereb Cortex 21:625–635.

Nimchinsky EA, Young WG, Yeung G, Shah RA, Gordon JW, Bloom FE, Morrison JH, Hof PR (2000) Differential vulnerability of oculomotor, facial, and hypoglossal nuclei in G86R superoxide dismutase transgenic mice. J Comp Neurol 416:112–125.

Novelli A, Reilly JA, Lysko PG, Henneberry RC (1988) Glutamate becomes neurotoxic via the N-methyl-d-aspartate receptor when intracellular energy levels are reduced. Brain Res 451:205–212.

Obál I, Engelhardt JI, Siklós L (2006) Axotomy induces contrasting changes in calcium and calcium-binding proteins in oculomotor and hypoglossal nuclei of Balb/c mice. J Comp Neurol 499:17–32.

Okamoto K, Hirai S, Amari M, Iizuka T, Watanabe M, Murakami N, Takatama M (1993) Oculomotor nuclear pathology in amyotrophic lateral sclerosis. Acta Neuropathol 85:458–462.

Paizs M, Engelhardt JI, Katarova Z, Siklós L (2010) Hypoglossal motor neurons display a reduced calcium increase after axotomy in mice with upregulated parvalbumin. J Comp Neurol 518:1946–1961.

Pambo-Pambo A, Durand J, Gueritaud J-P (2009) Early excitability changes in lumbar motoneurons of transgenic SOD1G85R and SOD1G(93A-Low) mice. J Neurophysiol 102:3627–3642.

Pardo CA, Xu Z, Borchelt DR, Price DL, Sisodia SS, Cleveland DW (1995) Superoxide dismutase is an abundant component in cell bodies, dendrites, and axons of motor neurons and in a subset of other neurons. Proc Natl Acad Sci USA 92:954–958.

Parone PA, Da Cruz S, Han JS, McAlonis-Downes M, Vetto AP, Lee SK, Tseng E, Cleveland DW (2013) Enhancing mitochondrial calcium buffering capacity reduces aggregation of misfolded SOD1 and motor neuron cell death without extending survival in mouse models of inherited amyotrophic lateral sclerosis. J Neurosci 33:4657–4671.

Patterson M, Sneyd J, Friel DD (2007) Depolarization-induced calcium responses in sympathetic neurons: relative contributions from Ca2+ entry, extrusion, ER/mitochondrial Ca2+ uptake and release, and Ca2+ buffering. J Gen Physiol 129:29–56.

Pieri M, Albo F, Gaetti C, Spalloni A, Bengtson CP, Longone P, Cavalcanti S, Zona C (2003) Altered excitability of motor neurons in a transgenic mouse model of familial amyotrophic lateral sclerosis. Neurosci Lett 351:153–156.

Pines G, Danbolt NC, Bjørås M, Zhang Y, Bendahan A, Eide L, Koepsell H, Storm-Mathisen J, Seeberg E, Kanner BI (1992) Cloning and expression of a rat brain L-glutamate transporter. Nature 360:464–467.

Powers RK, Binder MD (2003) Persistent sodium and calcium currents in rat hypoglossal motoneurons. J Neurophysiol 89:615–624.

Pun S, Santos AF, Saxena S, Xu L, Caroni P (2006) Selective vulnerability and pruning of phasic motoneuron axons in motoneuron disease alleviated by CNTF. Nat Neurosci 9:408–419.

Quinlan KA (2011) Links between electrophysiological and molecular pathology of amyotrophic lateral sclerosis. Integr Comp Biol 51:913–925.

Quinlan KA, Schuster JE, Fu R, Siddique T, Heckman CJ (2011) Altered postnatal maturation of electrical properties in spinal motoneurons in a mouse model of amyotrophic lateral sclerosis. The Journal of Physiology 589:2245–2260.

Redler RL, Dokholyan NV (2012) The Complex Molecular Biology of Amyotrophic Lateral Sclerosis (ALS), 1st ed. Elsevier Inc.

Regan RF, Choi DW (1991) Glutamate neurotoxicity in spinal cord cell culture. Neuroscience 43:585–591.

Rosen AD (1978) Amyotrophic Lateral Sclerosis: Clinical Features and Prognosis. Archives

of Neurology 35:638–642.

Rosen DR et al. (1993) Mutations in Cu/Zn superoxide dismutase gene are associated with familial amyotrophic lateral sclerosis. Nature 362:59–62.

Rothstein JD, Dykes-Hoberg M, Pardo CA, Bristol LA, Jin L, Kuncl RW, Kanai Y, Hediger MA, Wang Y, Schielke JP, Welty DF (1996) Knockout of glutamate transporters reveals a major role for astroglial transport in excitotoxicity and clearance of glutamate. Neuron 16:675–686.

Rothstein JD, Martin LJ, Kuncl RW (1992) Decreased Glutamate Transport by the Brain and Spinal Cord in Amyotrophic Lateral Sclerosis. N Engl J Med 326:1464–1468.

Rothstein JD, Patel S, Regan MR, Haenggeli C, Huang YH, Bergles DE, Jin L, Dykes Hoberg M, Vidensky S, Chung DS, Toan SV, Bruijn LI, Su Z-Z, Gupta P, Fisher PB (2005) Beta-lactam antibiotics offer neuroprotection by increasing glutamate transporter expression. Nature 433:73–77.

Rothstein JD, Tsai G, Kuncl RW, Clawson L, Cornblath DR, Drachman DB, Pestronk A, Stauch BL, Coyle JT (1990) Abnormal excitatory amino acid metabolism in amyotrophic lateral sclerosis. Ann Neurol 28:18–25.

Rothstein JD, Van Kammen M, Levey AI, Martin LJ, Kuncl RW (1995) Selective loss of glial glutamate transporter GLT-1 in amyotrophic lateral sclerosis. Ann Neurol 38:73–84.

Sasaki S, Iwata M (1996a) Dendritic synapses of anterior horn neurons in amyotrophic lateral sclerosis: an ultrastructural study. Acta Neuropathol 91:278–283.

Sasaki S, Iwata M (1996b) Impairment of fast axonal transport in the proximal axons of anterior horn neurons in amyotrophic lateral sclerosis. Neurology 47:535–540.

Schaefer AM, Sanes JR, Lichtman JW (2005) A compensatory subpopulation of motor neurons in a mouse model of amyotrophic lateral sclerosis. J Comp Neurol 490:209–219.

Schrøder HD, Reske-Nielsen E (1984) Preservation of the nucleus X-pelvic floor motosystem in amyotrophic lateral sclerosis. Clin Neuropathol 3:210–216.

Schwindt PC, Crill WE (1980) Properties of a persistent inward current in normal and TEA-injected motoneurons. J Neurophysiol.

Shaw PJ, Eggett CJ (2000) Molecular factors underlying selective vulnerability of motor neurons to neurodegeneration in amyotrophic lateral sclerosis - Springer. J Neurol 247 Suppl 1:I17–I27.

Shaw PJ, Ince PG (1997) Glutamate, excitotoxicity and amyotrophic lateral sclerosis. J Neurol 244:S3–S14.

Sherrington CS (1899) Address on the Spinal Animal. Medico-chirurgical transactions 82:449.

Sikl s LS, Engelhardt JZ, Harati Y, Smith RG, Jo F, Appel SH (1996) Ultrastructural evidence for altered calcium in motor nerve terminals in amyotrophc lateral sclerosis. Ann Neurol 39:203–216.

Siklos L, Engelhardt JI, Alexianu ME, Gurney ME, Siddique T, Appel SH (1998a) Intracellular calcium parallels motoneuron degeneration in SOD-1 mutant mice. J Neuropathol Exp Neurol 57:571–587.

Siklos L, Engelhardt JI, Alexianu ME, Gurney ME, Siddique T, Appel SH (1998b) Intracellular calcium parallels motoneuron degeneration in SOD-1 mutant mice. J Neuropathol Exp Neurol 57:571–587.

SLOB AK, OOMS MP, VREEBURG JTM (1980) PRENATAL AND EARLY POSTNATAL SEX DIFFERENCES IN PLASMA AND GONADAL TESTOSTERONE AND PLASMA LUTEINIZING HORMONE IN FEMALE AND MALE RATS. Journal of Endocrinology 87:81–87.

Sukiasyan N, Hultborn H, Zhang M (2009) Distribution of calcium channel Ca(V)1.3 immunoreactivity in the rat spinal cord and brain stem. Neuroscience 159:217–235.

Suzuki M, Tork C, Shelley B, McHugh J, Wallace K, Klein SM, Lindstrom MJ, Svendsen CN (2007) Sexual dimorphism in disease onset and progression of a rat model of ALS. Amyotroph Lateral Scler 8:20–25.

Tortarolo M, Crossthwaite AJ, Conforti L (2004) Expression of SOD1 G93A or wild-type SOD1 in primary cultures of astrocytes down-regulates the glutamate transporter GLT-1: lack of involvement of oxidative stress - Tortarolo - 2003 - Journal of Neurochemistry - Wiley Online Library. Journal of ….

Trotti D, Hediger MA, Rolfs A, Danbolt NC, Brown RH (1999) SOD1 mutants linked to amyotrophic lateral sclerosis selectively inactivate a glial glutamate transporter - Nature Neuroscience. Nat Neurosci 2:427–433.

Tsukita S, Ishikawa H (1980) The movement of membranous organelles in axons. Electron microscopic identification of anterogradely and retrogradely transported organelles. J Cell Biol.

Turner BJ, Talbot K (2008) Transgenics, toxicity and therapeutics in rodent models of mutant SOD1-mediated familial ALS. Prog Neurobiol 85:94–134.

Umemiya M, Berger AJ (1994) Properties and function of low- and high-voltage-activated Ca2+ channels in hypoglossal motoneurons. J Neurosci.

Urushitani M, Shimohama S, Kihara T, Sawada H, Akaike A, Ibi M, Inoue R, Kitamura Y, Taniguchi T, Kimura J (1998) Mechanism of selective motor neuronal death after exposure of spinal cord to glutamate: Involvement of glutamate-induced nitric oxide in motor neuron toxicity and nonmotor neuron protection. Ann Neurol 44:796–807.

Van Den Bosch L, Vandenberghe W, Klaassen H, Van Houtte E, Robberecht W (2000) Ca(2+)-permeable AMPA receptors and selective vulnerability of motor neurons. J Neurol Sci 180:29–34.

van Zundert B, Izaurieta P, Fritz E, Alvarez FJ (2012) Early pathogenesis in the adult-onset neurodegenerative disease amyotrophic lateral sclerosis. J Cell Biochem 113:3301–3312.

van Zundert B, Peuscher MH, Hynynen M, Chen A, Neve RL, Brown RH, Constantine-Paton M, Bellingham MC (2008) Neonatal neuronal circuitry shows hyperexcitable disturbance in a mouse model of the adult-onset neurodegenerative disease amyotrophic lateral sclerosis. J Neurosci 28:10864–10874.

Vanselow BK, Keller BU (2000) Calcium dynamics and buffering in oculomotor neurones from mouse that are particularly resistant during amyotrophic lateral sclerosis (ALS)-related motoneurone disease. The Journal of Physiology 525 Pt 2:433–445.

Veldink JH, Bär PR, Joosten EAJ, Otten M, Wokke JHJ, van den Berg LH (2003) Sexual differences in onset of disease and response to exercise in a transgenic model of ALS. Neuromuscul Disord 13:737–743.

Vivekananda U, Manjalay Z-R, Ganesalingam J, Simms J, Shaw CE, Leigh PN, Turner MR, Al-Chalabi A (2011) Low index-to-ring finger length ratio in sporadic ALS supports prenatally defined motor neuronal vulnerability. J Neurol.

Vucic S (2006) Novel threshold tracking techniques suggest that cortical hyperexcitability is an early feature of motor neuron disease. Brain 129:2436–2446.

Warita H, Itoyama Y, Abe K (1999) Selective impairment of fast anterograde axonal transport in the peripheral nerves of asymptomatic transgenic mice with a G93A mutant SOD1 gene. Brain Res 819:120–131.

Wong PC, Pardo CA, Borchelt DR, Lee MK, Copeland NG, Jenkins NA, Sisodia SS, Cleveland DW, Price DL (1995) An adverse property of a familial ALS-linked SOD1 mutation causes motor neuron disease characterized by vacuolar degeneration of mitochondria. Neuron 14:1105–1116.

Xu W, Lipscombe D (2001) Neuronal Ca(V)1.3alpha(1) L-type channels activate at relatively hyperpolarized membrane potentials and are incompletely inhibited by dihydropyridines. J Neurosci 21:5944–5951.

Zanette G, Tamburin S, Manganotti P, Refatti N, Forgione A, Rizzuto N (2002) Different mechanisms contribute to motor cortex hyperexcitability in amyotrophic lateral sclerosis. Clin Neurophysiol 113:1688–1697.

Zang DW, Yang Q, Wang HX, Egan G, Lopes EC, Cheema SS (2004) Magnetic resonance imaging reveals neuronal degeneration in the brainstem of the superoxide dismutase 1 transgenic mouse model of amyotrophic lateral sclerosis. Eur J Neurosci 20:1745–1751.

Zhang B, Tu P, Abtahian F, Trojanowski JQ, Lee VM (1997) Neurofilaments and orthograde transport are reduced in ventral root axons of transgenic mice that express human SOD1 with a G93A mutation. J Cell Biol 139:1307–1315.